Investigating Crater Lake Warming Using ASTER Thermal Imagery:
Case Studies at Ruapehu, Poás, Kawah Ijen, and Copahué Volcanoes

Laura E. Trunk

A thesis
submitted in partial fulfillment of the
requirements for the degree of

Master of Science

University of Washington

2005

Program Authorized to Offer Degree:
Earth and Space Sciences

University of Washington
Graduate School

This is to certify that I have examined this copy of a master's thesis by

Laura E. Trunk

and have found that it is complete and satisfactory in all respects,
and that any and all revisions required by the final
examining committee have been made.

Committee Members:

_____
Alan R. Gillespie

_____
Christopher G. Newhall

Date:_____

University of Washington

Abstract

Investigating Crater Lake Warming Using ASTER Thermal Imagery:
Case Studies at Ruapehu, Poás, Kawah Ijen, and Copahué Volcanoes

Laura E. Trunk

Chair of the Supervisory Committee:
Professor Alan Gillespie
Earth and Space Sciences

Crater lakes are unique in that they act as calorimeters, absorbing heat given off by intruding magma bodies, and integrating heat flow over space and time. Heat flowing out of the volcanic conduit under the lake causes an overall increase in the temperature of the lake. Thermal signals may precede eruptions and therefore, satellite observations of crater lake water temperatures may complement other methods currently used to monitor volcanic activity. A two-channel or split-window algorithm designed to correct for atmospheric conditions was applied to thermal images taken by the Advanced Spaceborne Thermal Emission and Reflection Radiometer (ASTER) of Lake Yugama on Kusatsu-Shirane volcano in Japan in order to measure the temperature of its crater lake. These temperature calculations were validated using lake water temperatures that were collected on the ground. Data from fieldwork undertaken in the summer of 2004 at Kusatsu-Shirane allow a comparison of ground-truth data with the radiant temperatures measured using ASTER imagery. Further images were analyzed of Ruapehu, Poás, Kawah Ijen, and Copahué volcanoes to acquire time-series of lake temperatures. Results, when considered in conjunction with traditional volcano monitoring techniques, lead to a better understanding of whether and how thermal changes in crater lakes aid in eruption forecasting.

TABLE OF CONTENTS

Page

i

LIST OF FIGURES

LIST OF TABLES

ACKNOWLEDGEMENTS

1. Introduction

1.1 Research Problem

Crater lakes are unique in that they act as calorimeters, absorbing heat given off by intruding magma bodies, and integrating heat flow over space and time. Heat flowing out of the volcanic conduit under a crater lake causes an overall increase in the temperature of the lake and trends in lake temperature therefore reflect activity of the magmatic intrusions below them. Can the patterns of lake warming, in response to this heat flux, observed by satellites help us to predict volcanic activity? To answer this question, we need to explore how the temperatures of crater lakes respond to magmatic intrusion, including how soon before an eruption occurs a noticeable temperature increase may be observed and how much warming must be present in order for it to be observable using satellite imagery. Determining how quickly crater lakes respond to the heat flux from intruding magma and how soon before eruption thermal signals may be seen could provide time constraints on magma intrusion.

1.2 Why Crater Lakes?

Of the approximately 700 active volcanoes in the world, roughly 12% have crater lakes (Rowe et al., 1992). Eruptions of these volcanoes can cause serious loss of life and property. However, these eruptions do not occur without warning. Seismicity, deformation, changes in gravity, lake water chemistry, and lake water temperatures may indicate that an intrusion is taking place (Rowe et al., 1992; Giggenbach, 1994; Ohba et

al., 2000). Why is it more meaningful to study the surface temperature of water in crater lakes rather than the surface temperature of the ground of the volcano? Because most of the heat flow is accomplished by the convecting hydrothermal system, heat flow mainly occurs along fissures. Where the heat makes its way to the surface, it is localized along these cracks, where it escapes as steam from hot springs and fumaroles. Many of these heat sources feed directly into crater lakes, which integrate incoming heat flow over space and time. Heat flowing out of the volcanic conduit under the lake causes an overall increase in the temperature of the lake.

Crater lake temperatures calculated from thermal images may complement other methods currently used to monitor volcanic activity. In some instances, lake temperatures have increased before an increase in seismicity or before deformation of the edifice. When magma intrusion is slow and/or deep, deformation and seismicity may be very subtle and hard to detect. However, hot CO_2 gas can begin to leak from magma at that depth, up into the hydrothermal system.

Changes in lake chemistry, such as increases in Mg, Cl, or SO_4 concentrations have also been observed prior to eruptions, as acidic gases are absorbed into groundwater and into the lake. Temperature, acidity, and species that are dissolved from country rock by the acid (e.g., Mg) tend to increase together.

1.3 Advantages of Remote Sensing

Remote sensing has been used in numerous ways to monitor volcanic activity. Satellite images have been used to detect eruption plumes that pose a threat to aircraft, for

thermal studies of lava at the surface, to monitor deformation of volcanic edifices, to make high resolution topographic maps for use in calculating volume or predicting flow paths of erupted materials, and to determine the distribution of erupted materials (Mouginis-Mark and Domergue-Schmidt, 2000).

Remote sensing of crater lakes offers several advantages over in-situ field studies. First, it is safer, especially during times of volcanic unrest. Second, the logistics of visiting crater lakes can be formidable and costly, so in-situ measurements are typically infrequent. Third, by use of remote sensing, a small research group can monitor many lakes, and then pass results to the responsible local volcano observatories. Overall, remote observations save time, money, and possibly lives.

2. Theoretical Background

2.1 Past Observations of Crater Lake Warming

Crater lake warming has been observed in numerous cases prior to eruptions. Some examples include the 1966, 1968, and 1971 eruptions of Ruapehu volcano in New Zealand (Oppenheimer, 1993), the 1971 eruption of Soufriére St. Vincent (Shepherd and Sigurdsson, 1978), the 1989 eruption of Costa Rica's Poás volcano (Brown et al., 1989; Brown et al., 1991; Rowe et al., 1992; Rymer and Cassidy, 2000), the 1989 eruption of Kusatsu-Shirane volcano in Japan (Ohba et al., 2000), the 1990 eruption of Kelut volcano in Java, Indonesia (Badrudin, 1994; Lesage, 1995; Vandemeulebrouck et al., 2000), and the 2000 eruption of Copahué volcano on the Argentinean-Chilean border (Varekamp, 2001).

One well-known case where water temperatures rose significantly prior to eruption is that of Kelut Volcano in Indonesia. As can be seen in figure 2.1, over a period of 4 months preceding the February 1990 eruption, water temperatures at the summit lake increased from approximately 31 to 38 ºC (Badrudin, 1994).

Similarly, temperatures of the crater lake at Kusatsu-Shirane Volcano in Japan increased over a period of several months in late 1989 from 9 to 12 ºC. In this case, the heating was not followed by an eruption. However, the high level of seismicity associated with the warming indicated that an intrusion was underway, which must have stalled prior to eruption (Ohba et al., 1994).

2.2 Principles of Crater Lake Warming

Crater lakes are the surface expressions of the complex hydrothermal systems overlying magma bodies beneath volcanoes. Certain conditions must be fulfilled in order for hot crater lakes to exist. There must be a high water supply in a crater with low permeability, beneath which there is effective sub-surface heat transport (Brown et al., 1989). Water mass balance, with inputs of meteoric water and geothermal vapor or liquid and outputs of water lost by evaporation, seepage, or stream outflow determines whether a lake will maintain its volume or be growing or shrinking at any given time (Brantley et al., 1993). In order for lake water temperature to increase, the amount of heat entering the system must be greater than the amount that is outgoing. Pasternack and Varekamp (1997) developed a simple box model to apply to the heat budget of crater lakes.

$$(1) \quad E_{cond}^{volc} + E_{rad}^{sun} + E_{volc} + E_{rad}^{atm} = E_{rad}^{lake} + E_{evap} + E_{cond}^{lake} + E_{meteoric}$$

This shows that the sum of the conductive heat input from a shallow magma body (E_{cond}^{volc}), the short-wavelength solar flux (E_{rad}^{sun}), the enthalpy of the volcanic flux, or convective input from magmatic gases or hot brines (E_{volc}), and the long-wavelength radiative input from the atmosphere (E_{rad}^{atm}) must equal the lake surface long-wavelength radiation (E_{rad}^{lake}), heat loss due to lake surface evaporation (E_{evap}) and lake surface conduction (E_{cond}^{lake}), and heat used to warm meteoric influxes up to the lake's temperature ($E_{meteoric}$). Figure 2.2 summarizes these heat and mass fluxes. Smaller lakes can be expected to respond more rapidly to increased heat flux than large lakes because they have less buffering capacity. Regardless of size, a lake cannot exist for long in any case

where high thermal input requires the lake to dissipate so much heat through evaporation and radiation that precipitation cannot replace the lost mass (Pasternack and Varekamp, 1997).

2.3 Mechanisms of Heat Transfer and Examples

How is heat transferred from the intruding magma body to a crater lake in order to cause a thermal response? First, heat must be transferred from the intrusion, through the hydrothermal system, and into the lake. Then, heat transfer must occur within the lake in order for warming to be seen at the lake surface. Hurst et al. (1991) define four regions that are important in the transfer of heat from intrusion to lake: the magma body and its boundary layer, the volcanic conduit, a boundary layer at the top of the conduit beneath the lake, and the bottom waters of the lake itself. Heat transfer is accomplished by multiphase convective flow or through a heat-pipe mechanism, and conduction accounts for an insignificant fraction of total heat flow (Pasternack and Varekamp, 1997).

Convection, the dominant heat-transfer mechanism, involves the loss of enthalpy from rising magmatic gases or hot brines (Brown et al., 1989). Magmatic steam, which may or may not be superheated, has an enthalpy of around 3.0 MJ/kg, making this an efficient means of heat transport (Hurst et al., 1991). However, in some cases, heat loss from magmatic steam alone cannot account for the high ratios of energy to mass input into crater lakes. The "heat-pipe" mechanism proposed by Hurst et al. (1991) allows for heat transport without a net transport of mass. In their model, a hot vapor phase moves upward from the magma body towards the surface, cools, and condenses, releasing its

heat before it sinks back down to be reheated (figure 2.3). Because vaporization of fluid occurs when the vapor pressure equals the total pressure at depth (Casertano et al., 1987), heat-pipes may be either liquid- or vapor-dominated. The heat-pipe model has been used to explain heat transfer in many different geothermal systems. One example is the case of Ruapehu volcano, where up to half of all heat transfer may be accomplished through a heat-pipe (Kusakabe, 1996).

Once heat reaches the bottom of a crater lake, it still must be transferred into the water and distributed throughout the lake volume. The bottom waters of crater lakes are composed of layers of immiscible liquids or suspensions through which heat travels by convection (Hurst et al., 1991). Many crater lakes have a layer of liquid sulfur on the bottom, formed when H_2S is oxidized by SO_2 or O_2. Because of its relatively high specific gravity of 2.0, this sulfur settles to the lake bottom, where it accumulates, heats, and melts (Giggenbach, 1974). These sulfur layers may add heat to the water via a conductive heat flux (Pasternack and Varekamp, 1997).

Heat may be transferred throughout the lake by either wholesale convection driven by heat entering at various locations on the bottom, or by the action of a hot buoyant jet originating from a primary vent (Pasternack and Varekamp, 1997). Free thermal convection occurs when the bottom layers of water are heated, expand, become lighter than the top layers, and rise due to buoyancy contrast, delivering their heat to the surface. Plumes originating from hot vents entrain cold water as they rise and are particularly effective at warming surface waters quickly as the hot water spreads out over the lake surface (Hurst and Dibble, 1981). Magmatic gases, such as CO_2, entering the

lake may pass right through without major loss of enthalpy, but may still contribute to the distribution of heat by creating turbulence that allows hot water to mix with the cold (Giggenbach, 1974).

Casertano et al. (1987) performed a series of simple lab experiments to simulate heat transfer in a volcanic conduit beneath a crater lake. A cylindrical container was filled with rock samples of varying grain sizes from Poás volcano, covered with water, and set on a plate heated to 200 ºC. For one trial, the material was packed by allowing it to dry. After warming, convection started and small, vertical, permeable channels formed in the sediment. Water inside the sample reached the boiling point and trapped steam created a horizontal cavity in the material, giving rise to occasional upwards bursts and the release of plumes into the overlying water (figure 2.4a). The results of the second experiment might more accurately represent the response of a real volcanic system, since the rocks were loosely packed, analogous to the poorly consolidated rubble that fills volcanic conduits. Again, convection started in response to warming. This time, more vertical channels formed between the heat source and the convection cells, which were at around the boiling point, and plumes entered the water from the cells regularly (figure 2.4b).

The preceding discussion summarizes simple transport of heat from magmatic intrusion to lake surface. However, complete heat transport models must also account for variations in the magmatic activity and for magma-water interaction (termed FCI, or fuel-coolant interactions) and vesiculation, both of which can fragment the magma and speed heat transfer. Increasing exsolution and release of gas as magma rises must also be

considered. A number of researchers have carried out studies to explore the mechanisms of heat transfer in evidence at active volcanoes. Some especially well-studied cases are Kelut, Kusatsu-Shirane, Poás, and Ruapehu volcanoes and these are presented here as real-world examples.

2.3.1 Kelut Volcano (1989-1990)

The first sign of renewed activity at Kelut volcano was an increase in the level of low-frequency acoustic noise about one year before the 1990 eruption. This signal has been attributed to boiling at depth within the hydrothermal system and marked the onset of heat transfer from the magmatic intrusion. Heating of the hydrothermal system continued for seven months before other signs of unrest – increased seismicity, changes in lake water chemistry (increasing concentrations of sulfate, boron, magnesium, chloride, and an increasing Mg/Cl ratio), and warming of the crater lake – were noted. The increase in crater lake water temperature showed that over-pressurization of the system had resulted in hydraulic fracturing of the low-strength plug that blocked the conduit, allowing heat to be transferred convectively to the surface. High-frequency acoustic noise increased at this point, the sound being that of volcanic gases bubbling through the lake in a convective column. Heating of the lake continued as the aquifer beneath it warmed, although both heating and high-frequency acoustic noise slowed prior to the eruption due to geothermal self-sealing of cracks. Initial phreatic eruptions were followed on 10 February 1990 by a magmatic eruption (Badrudin, 1994; Lesage, 1995; Vandemeulebrouck et al., 2000).

2.3.2 Kusatsu-Shirane Volcano

Lake Yugama is a crater lake atop the summit of Kusatsu-Shirane volcano. Yugama, which translates to "hot-water cauldron," is thoroughly mixed by convection, two main vents are located on the lake bottom, where molten sulfur pools exist with a temperature of around 126 ºC, and a column of bubbles rises above each. It has been postulated that a shallow vapor-liquid reservoir exists beneath the lake, formed when meteoric water boils and combines with HTVG (high-temperature volcanic gases) from the magma body. This reservoir, at a temperature of 197 ºC, supplies heat to the lake when the liquid phase enters the lake through the bottom vents. The vapor portion of the parental fluid is discharged from fumaroles on the flanks of the volcano (figure 2.5) (Ohba et al., 1994; Ohba et al., 2000; Tsuya, 1932).

2.3.3 Poás Volcano (1980-81, 1986-89)

Below Poás volcano, a magma body at a depth of 500 m, probably emplaced during 1953 eruptive activity, supplies heat to the overlying hydrothermal system. Heat conducts from the magma, across a chilled margin, and into the vapor-dominated heat-pipe above. This heat-pipe moves enough heat to drive strong convection in the liquid-dominated region beneath the crater lake. The crater lake is thermally well mixed; a 1988 study by Neshyba et al. showed that near-surface temperatures varied by only 1.4 ºC across its surface and the patches of turbulence in evidence most of the time indicate that convection is taking place, probably in the form of a single convection cell. In the usual

case, the lake dissipates heat efficiently enough through surface evaporation to maintain a steady temperature (Casertano et al., 1987; Brown et al., 1989; Rowe et al., 1992).

The 1980-81 activity began with seismic activity in the form of A-type earthquakes in July of 1980. These earthquakes were caused by brittle fracture of the magma carapace, which allowed hydrothermal fluids to percolate in and be heated. The convection of these hot fluids transports heat away from the magma with 3 to 5 times the efficiency of conduction. This first seismicity was followed by B-type earthquakes and harmonic tremor, as HTVG were degassed from the magma. Temperatures of fumaroles in the area of the dome increased and a decrease in the local magnetic field indicated that hot material had intruded beneath it. Lake water temperature did not increase until the end of 1981, and lake level remained unchanged throughout the active period (Casertano et al., 1987; Rowe et al., 1992; Rymer and Cassidy, 2000).

In early 1986, an increase in A-type seismicity was again followed by increasing numbers of B-type events and volcanic tremor. In this case, an increase in micro-gravity on the crater floor showed that activity was centered beneath the crater lake. Because the size of intrusion implied by the gravity anomaly was not large enough to account for the resulting increase in lake temperature, dendritic intrusions supplied by a deeper magma feeder system were invoked, with convection of the deep magma body supplying hot buoyant material to the dendritic intrusions, which transfer heat and HTVG to the hydrothermal system as they pushed upwards through cracks and fissures. An increase in F, Cl, and S fluxes supports the involvement of fresh magma. The increased heat supplied by the intrusions resulted in a more efficient hydrothermal heat transfer and led

to increased evaporation from the crater lake. When the lake temperature reached 65 ºC

in mid 1987, geysering began. Further heating dried the lake completely, and the activity

culminated in a dry eruption of non-juvenile ash in April of 1989. Figure 2.6 summarizes

this model of the Poás system (Brown et al., 1991; Rowe et al., 1992; Rymer and

Cassidy, 2000).

2.3.4 Ruapehu Volcano (1995)

The temperature of Ruapehu's Crater Lake has been measured at least monthly

since the 1960's. The lake is well mixed, with the surface temperature constant to within

± 1.0 ºC around the lake (see figure 2.7 for a model mixing within the lake).

Heat is supplied to Crater Lake through a combination of convection and a heat-

pipe. Typically, the lake undergoes heating cycles on the order of 6 to 15 months. The

lake temperature may increase for a period of 1 to 2 months, and then decrease over the

next 6 months to one year. These cycles seem to indicate that the 6 m thick layer of

liquid sulfur at the bottom of the lake acts as a partial barrier to heat transport. When the

sulfur temperature is less than 160 ºC, its viscosity is low enough that it flows easily and

hot water and HTVG may easily pass through the layer. Above 160 ºC, however, the

viscosity increases and heat is only able to pass into the lake by conduction through the

sulfur, so heat supply is greatly reduced. Eventually, enough heat builds up beneath the

lake to warm the sulfur to a point where its viscosity again decreases (figure 2.8) and hot

gases may again pass though (Hurst et al., 1991; Scott, 1991; Christenson, 1994; Hurst

and McGinty, 1999).

To explore how the magmatic/hydrothermal system functions during volcanic activity at Ruapehu, it is useful to study the eruption of September 1995. HTVG from rising magma caused the temperature of Crater Lake to increase beginning in January of 1995, and was accompanied by an increase in seismicity. Coincident with the second burst of seismic activity in April of 1995 was an increase in the Mg/Cl ratio of the lake water, indicating that magma had made contact with the water of the hydrothermal system. The lake temperature increased further and a small eruption occurred through the lake on 26 April 1995. Activity stalled between June and August of 1995, and the lake temperature decreased, probably because the top of the intrusion had been quenched and was acting as a barrier to heat transport. By mid-September however, further intrusion pushed the magma through the liquid sulfur on the lake bottom and phreatomagmatic eruptions began. The graphs of figure 2.9 show the trends in lake water temperature, Mg/Cl ratio, and the earthquake activity throughout 1995 (Hurst and McGinty, 1999; Christenson, 2000).

2.4 The Skin Effect

When measuring water temperatures radiometrically, one factor that must be considered is the "skin effect." Traditional ground-based temperature measurements using contact thermometers record "bulk" water temperature, necessarily the temperature at some depth below the air-water interface. Bulk water temperature may be measured at any depth, including at the near surface. However, "surface" temperature and "skin" temperature are not synonymous. Skin temperature is taken to mean the temperature of

the top 0.1 mm of water, that which is observed by radiometers. This is an important

distinction because, for various reasons, skin temperature may vary from bulk surface

temperature by several tenths of a degree or even by a few degrees Celsius (Robinson et

al., 1984; Oppenheimer, 1997a; Oppenheimer, 1997b).

The skin effect is caused by vertical heat flux at the air-water interface. When

there is a net heat loss through the surface (Q_n), the skin temperature (T_s) becomes cooler

than the bulk temperature (T_b). Two possible mechanisms exist for heat transfer at the

water surface: free and forced convection. Free convection is buoyancy-driven; the skin

is cooler than the underlying water and gravity causes it to sink. Forced convection is

driven by shear stress on the surface, by wind. Under zero wind conditions, free

convection alone operates and a skin-bulk temperature deviation (ΔT_{b-s}) of less than one

1 °C is possible (Robinson et al., 1984; Oppenheimer, 1997a).

The skin effect is variable and depends on many factors in addition to Q_n (which

itself depends on ambient air temperature and humidity). Oppenheimer (1997a) found

the following empirical relationship between ΔT_{b-s} and windspeed, based on fieldwork at

Kawah Ijen volcano in Indonesia:

$$(2) \quad \Delta T_{b-s} = 1.12 + 0.16 u_1$$

where u_1 is the windspeed at 1 m height. While this relation is not directly applicable to

other lakes due to their different bulk temperature and ambient temperature conditions, it

does illustrate how windspeed may increase the ΔT_{b-s}. At windspeeds greater than 3 m/s,

the surface skin is disturbed and this relation no longer holds. In general, the effect that

solar heating has in warming the skin is decreased by increasing windspeed (Robinson et al., 1984; Hasse, 1971; Oppenheimer, 1997a).

Surface slicks, when they are present, may also influence $\Delta T_{b\text{-}s}$, although in ways that are hard to predict. In the case of crater lakes, sulfur may be floating on the water surface. Overall, this would serve to lower the emissivity of the surface, reducing the apparent skin temperature. Rafts of sulfur could insulate the lake from the cooling effects of the wind that would otherwise counteract solar warming and thereby increase $\Delta T_{b\text{-}s}$. Or, they could inhibit heat loss by preventing evaporation, which would serve to decrease the skin-bulk temperature deviation (Robinson et al., 1984).

Finally, cloud cover (or, in the case of crater lakes, steaming from the lake surface) serves to increase the amount of downwelling radiation, causing the skin temperature to increase. This effect can hopefully be avoided by selecting clear images, although sub-visible cover may be overlooked (Robinson et al., 1984).

Several researchers have attempted to quantify the skin effect through detailed field observations and laboratory experiments (see Robinson et al., 1984 for a review). These range from simple measurements made on a calm pond at night with a mercury thermometer to experiments carried out under controlled laboratory conditions using sophisticated radiometers. Reported results range from $\Delta T_{b\text{-}s} = -3.4$ to $+ 5.0$ ºC under the most extreme conditions (high winds, oil slicks, etc). Under less extreme conditions, most show variations of 0.2 to 0.5 degrees (Robinson et al., 1984).

Hook et al. (2003) made near-continuous measurements of radiometric skin temperatures and bulk temperatures for Lake Tahoe, over a range of water temperatures

from 5 – 22 ºC. They found the average daytime and nighttime skin temperatures to be

0.11 and 0.46 ºC cooler, respectively, than bulk temperatures. Figure 2.10 shows how

skin and bulk temperatures varied over an example 24-hour period at Lake Tahoe.

Further studies of the skin effect have been carried out for cooling ponds, which

make better analogues for crater lakes than Lake Tahoe because of their high

temperatures. Table 2.1 summarizes some of the skin-bulk temperature deviations that

have been observed for cooling ponds at different temperatures (Oppenheimer, 1997a).

Finally, fieldwork carried out by Oppenheimer (1997a) at Kawah Ijen revealed a

range of 0.3 – 3.4 ºC for ΔT_{b-s}, with the average being $\Delta T_{b-s} = 1.5$ ºC for the lake, which

had a bulk temperature of 43.1 ºC.
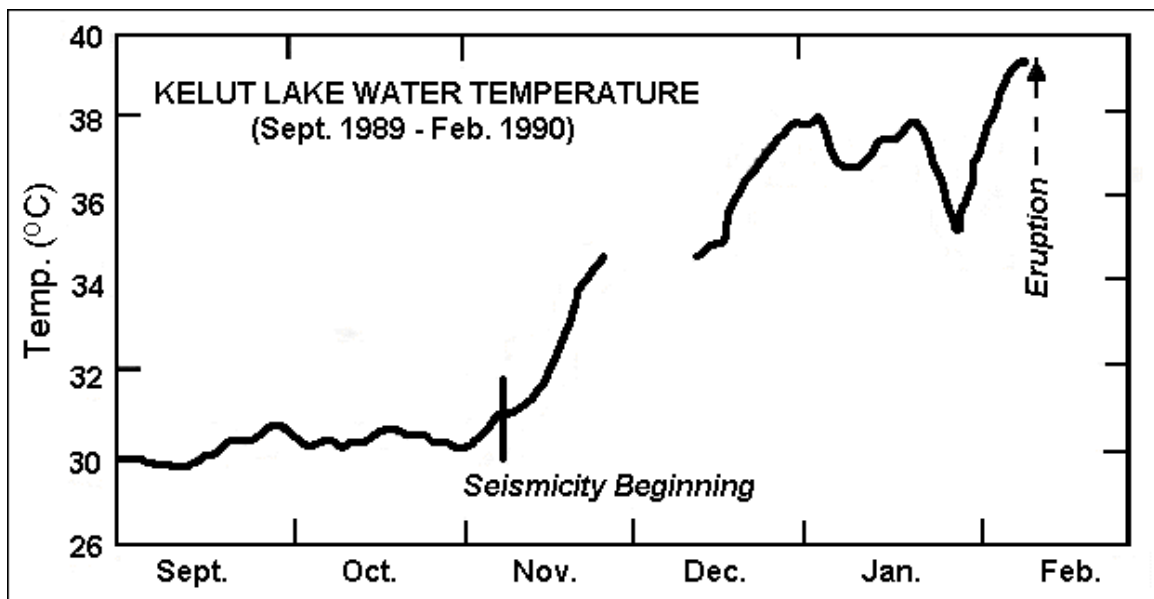
Figure 2.1 Continuous temperature record of the Kelut crater lake Sept. 1989 – Feb.1990
(Badrudin, 1994).
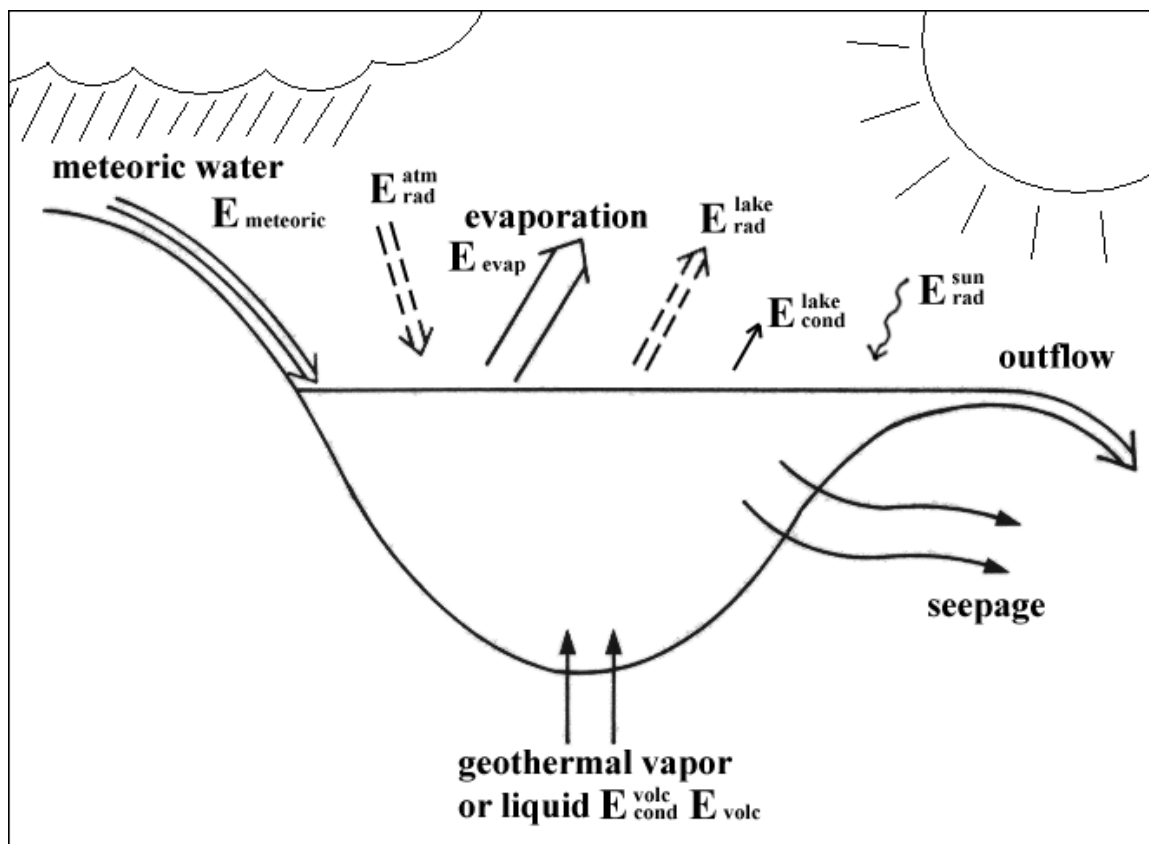
Figure 2.2 Diagram summarizing the mass and energy balance of crater lakes (modified from Hurst et al., 1991).
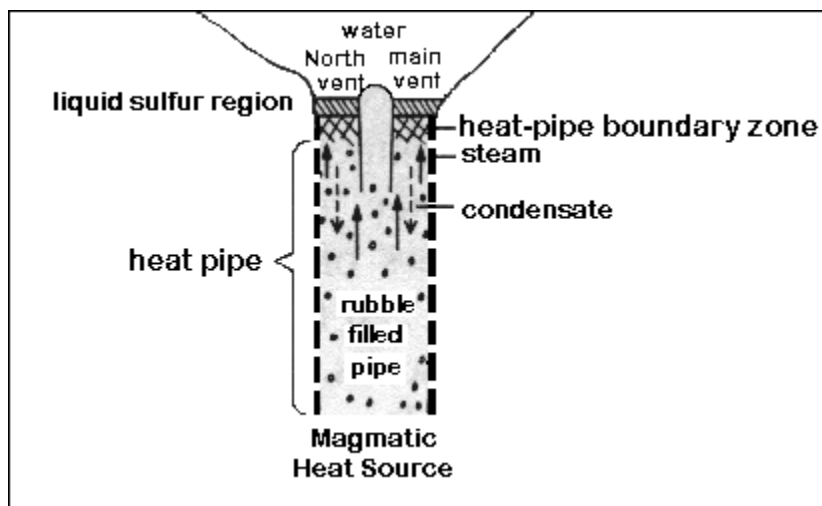
Figure 2.3 Cross-section diagram illustrating the heat-pipe model for Ruapehu volcano (Hurst et al., 1991).
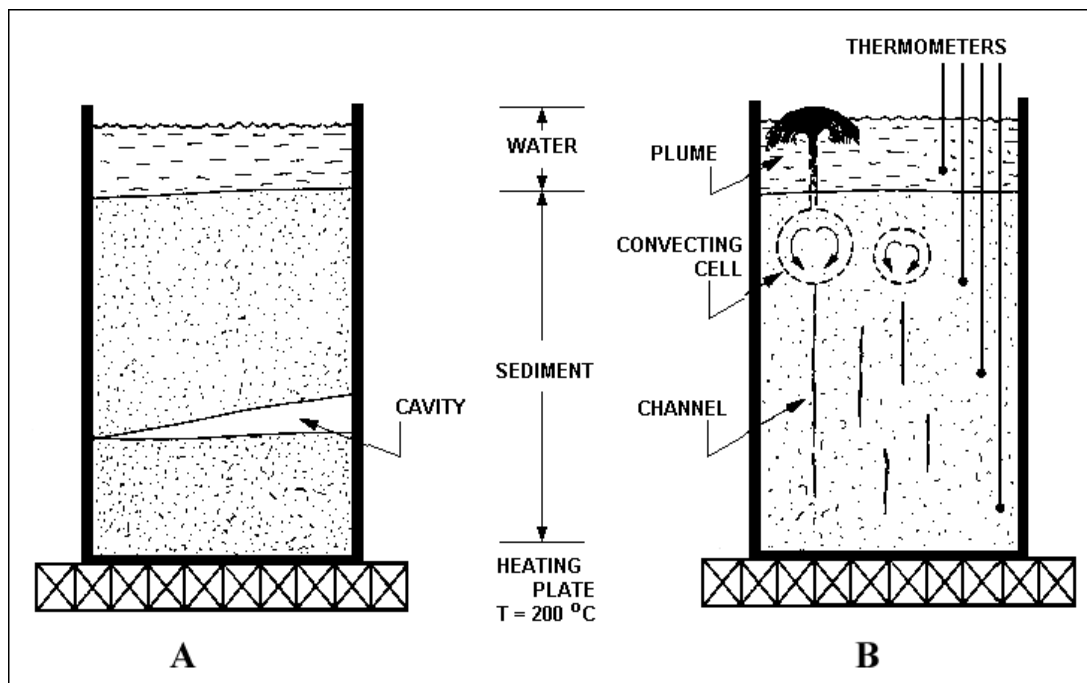
Figure 2.4 Casertano et al.'s experiments in a) Poás volcano sediments packed by desiccation and b) unconsolidated volcanic material (Casertano et al., 1987).
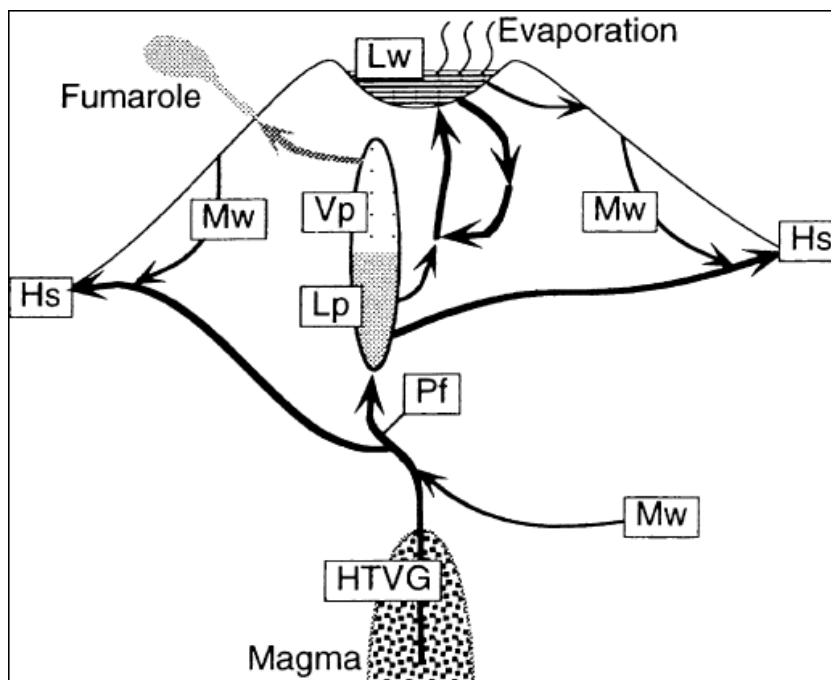
Figure 2.5 Model of the hydrothermal system beneath Yugama Lake. Lw = lake water, Mw = meteoric water, HTVG = high-temperature volcanic gases, Pf = parental fluid, Lp = liquid phase, Vp = vapor phase, Hs = hot springs (from Ohba et al., 2000).
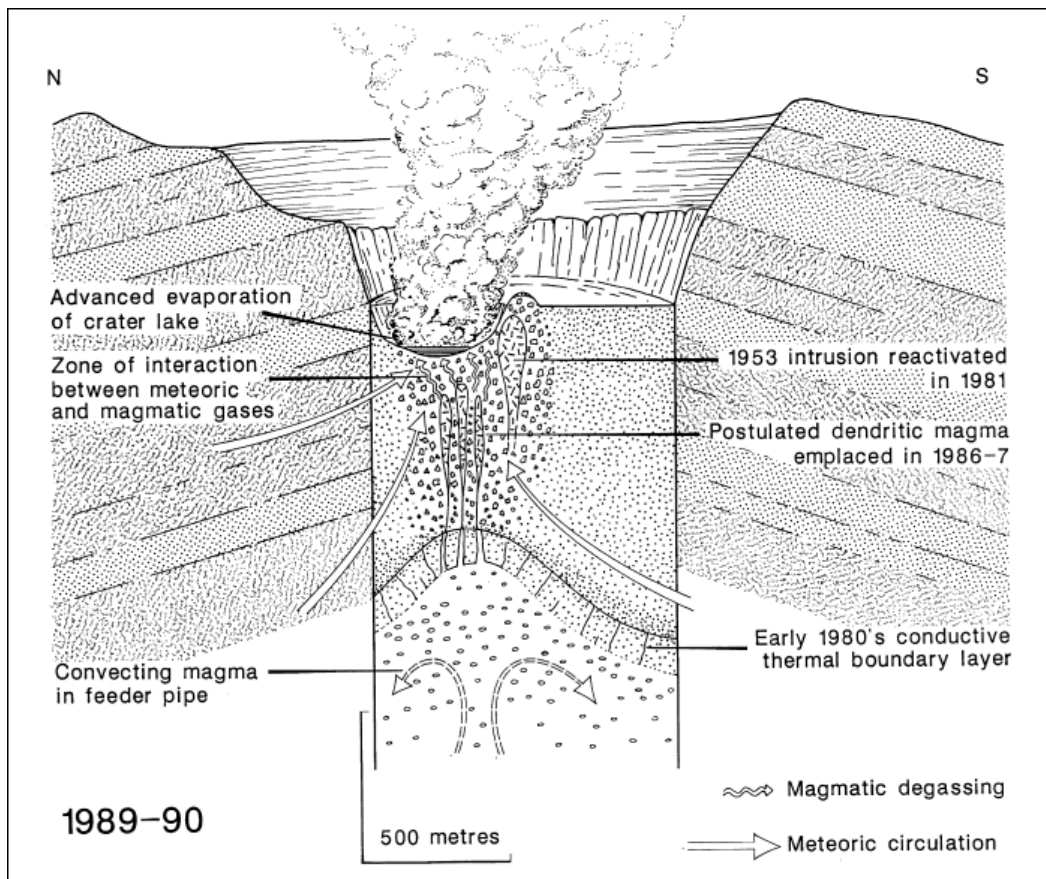
Figure 2.6 Diagram of the model proposed for Poás volcano's magmatic and hydrothermal system (Rymer and Cassidy, 2000).
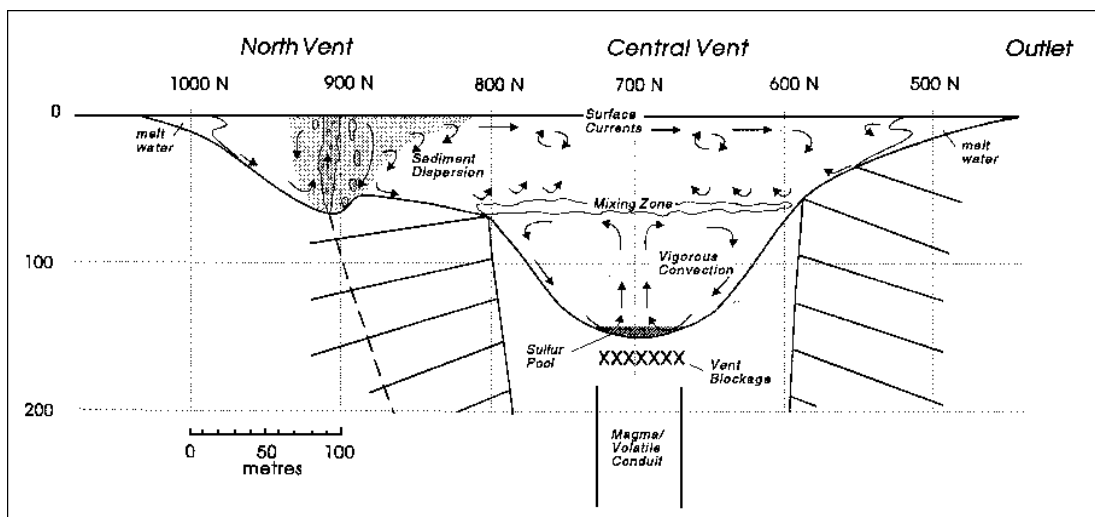
Figure 2.7 Schematic illustration of mixing within Crater Lake, Ruapehu volcano (Christenson, 1994).
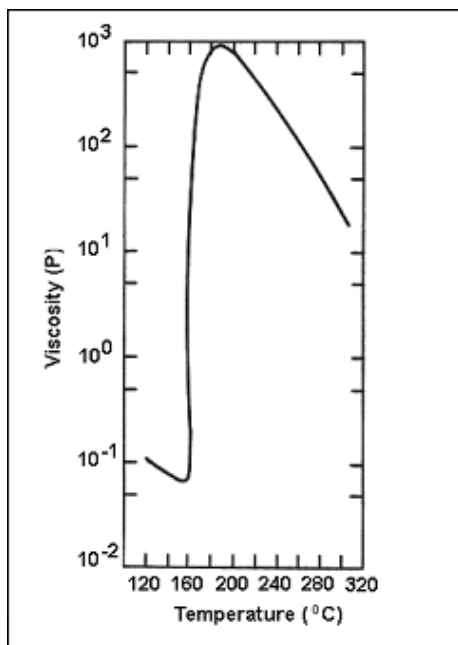
Figure 2.8 Variation of sulfur viscosity with temperature (Hurst et al., 1991).
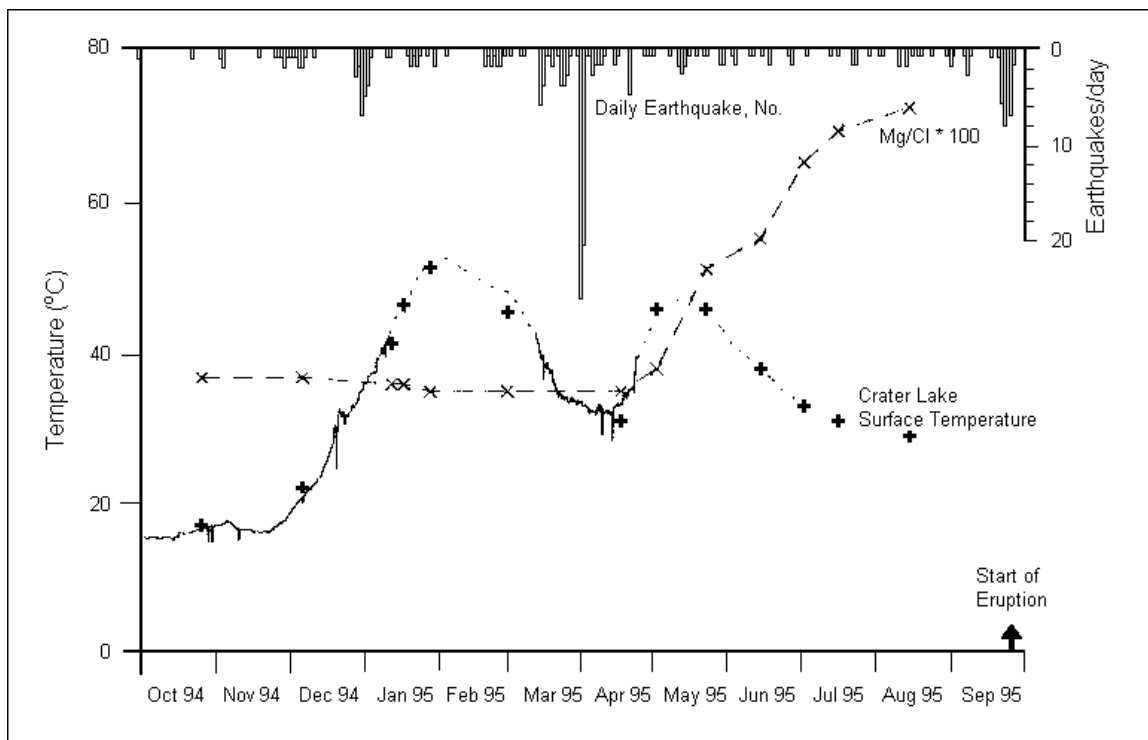
Figure 2.9 Graph showing Crater Lake temperature, Mg/Cl ratio, and number of earthquakes prior to the Sept. 1995 eruption of Ruapehu volcano (after Hurst and McGinty, 1999).
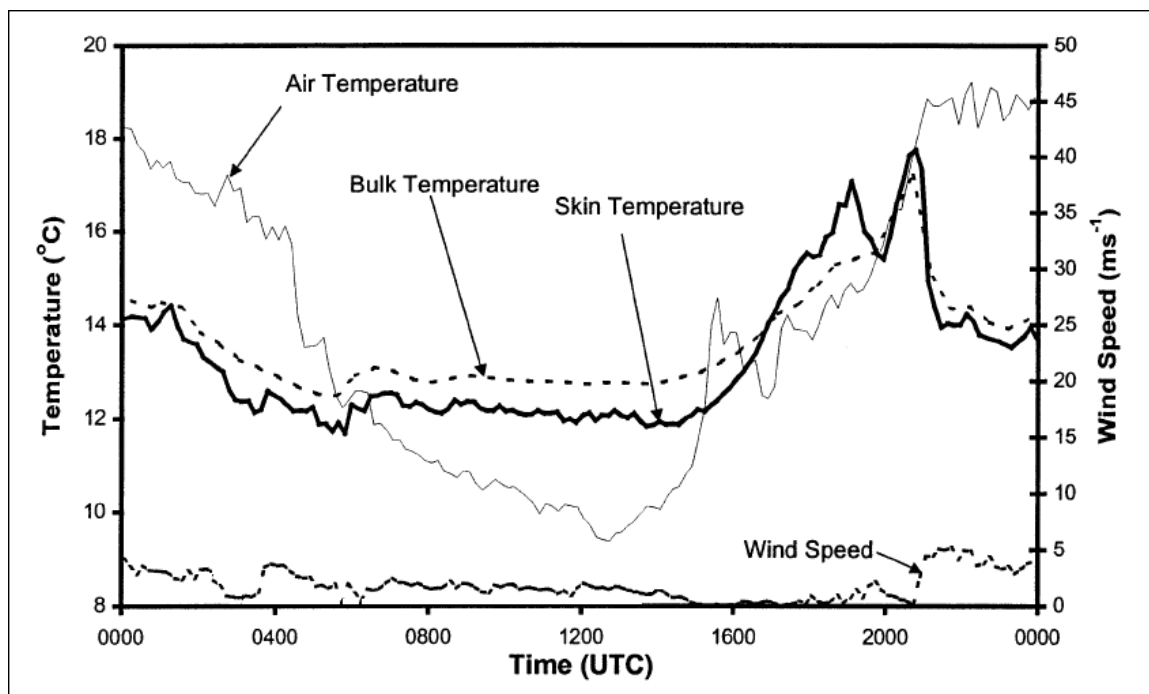
Figure 2.10 Skin, bulk, and ambient air temperatures for Lake Tahoe on 7 Jun 2001. Note that 1400 UTC is 6 a.m. local time. A decrease in ΔT_{b-s} corresponds to the increase in wind speed around 2100 UTC (Hook et al., 2003).

Table 2.1 Skin-bulk temperature deviation for cooling ponds at different temperatures (data from Oppenheimer, 1997a)

T_b	range of ΔT_{b-s} (°C)	average ΔT_{b-s} (°C)
35 °C	0.1 – 2.3 °C	0.8 °C
up to 37.5 °C	0.3 – 1.5 °C	-
70 °C	0.2 – 3.7 °C	1.8 °C

3. Method

3.1 Overview

A variety of methods have been explored in order to determine water temperatures from thermal satellite imagery. The main difficulty in calculating accurate temperatures is that moisture in the atmosphere both absorbs radiance emitted by the land and emits radiance in all directions, respectively reducing and increasing the temperatures calculated from "at-satellite" radiances. Other difficulties are also present in using radiant temperatures to represent kinetic lake temperatures. Thus, radiant temperature may not be an accurate representation of the kinetic temperature of the lake surface due to factors such as wind, and the surface temperature may differ from the overall temperature of a lake if the lake is thermally stratified or contains lateral temperature variations.

Thermal images taken by the Advanced Spaceborne Thermal Emission and Reflection Radiometer (ASTER) were obtained for several volcanoes with crater lakes. For each image, the pixels corresponding to the crater lake were selected and the lake water temperature was calculated using a split-window algorithm, which was designed to eliminate atmospheric effects. These split-window temperatures were then compared to existing ground-based temperature measurements, or "ground-truth," to determine the usability of the method. Fieldwork was also carried out at Yugama Lake on Kusatsu-Shirane volcano in order to investigate the relationship between radiant temperature, surface kinetic temperature, and temperature at depth for an example lake.

3.2 ASTER Thermal Imagery

3.2.1 ASTER Instrument Characteristics

The ASTER sensor is part of NASA's Earth Observing System (EOS) Terra satellite platform, which was launched December 18, 1999 (Pieri and Abrams, 2004). ASTER has the unique ability to collect multispectral data in the thermal infrared (TIR) region of the spectrum, with five bands in the TIR region of the spectrum (Table 3.1): bands 10 to 14, at 8.30, 8.65, 9.10, 10.6, and 11.3 μm, respectively (Yamaguchi et al., 1998). Theoretically, the noise equivalent temperature difference (NEΔT) is 0.3 K for ASTER in the TIR (Tonooka et al., 2004). Practically, the absolute radiometric accuracy for the TIR bands is ±1 K or less in the 270 – 340 K range, where lake water temperature typically fall (Yamaguchi et al., 1998). With a spatial resolution of 90 meters in the TIR, ASTER can "see" a pure water pixel and therefore be used to measure the temperature of lakes greater than 250 m in diameter (Oppenheimer, 1996).

3.2.2 ASTER Image Data

ASTER data are processed and distributed in the form of many different products intended for different applications (figure 3.1). Raw satellite data are referred to as the Level-0 product, which consists of the radiance for each spectral band, as well as supplemental instrument data and spacecraft ancillary data. These raw data are processed by the Japanese Ground Data System (GDS) into the Level-1A product, which consists of radiometric coefficients and geolocation data in addition to the image data and auxiliary data. Finally, the Level-1A data are processed to Level-1B data, the radiometrically

calibrated and geometrically registered "radiance-at-sensor" product from which all

higher-level products are made (Fujisada et al., 1996).

For this study, the Level-2 Brightness Temperature At Sensor product (ASTER

product number AST04) was used. This product is produced on-request by the Land

Processes Distributed Active Archive Center (LPDAAC) from Level-1B data. Data in

the AST04 product are presented in degrees Celsius, scaled by a factor of 100. These

temperatures are not corrected for atmospheric effects, but are merely calculated from the

sensor radiance using the inverse Planck function and assuming a surface emissivity of

1.0 (as though the emitting object is a perfect blackbody) (Alley and Jentoft-Nilsen,

1999).

3.2.3 Acquiring Images

ASTER travels in a sun-synchronous, near-polar orbit, and has the ability to

collect a daytime image with data in both the visible and TIR over every point on Earth at

least once every 16 days. Because TIR data can also be obtained at night, TIR images

can be taken for each point at least every 8 days and more often at higher latitudes

(Oppenheimer, 1993). However, because of data-volume and communications

limitations, images are only taken for locations of interest. The ASTER science team

guides the acquisition of images, although individual researchers may request to have

data acquired for specific targets using Data Acquisition Requests (DAR's). Because

volcano monitoring is part of the primary science objective of the ASTER mission, many

images have been taken of volcanoes since the launch of the satellite. A database of

these archived images is maintained by LPDAAC and can be accessed through the EOS

Data Gateway website (http://edcimswww.cr.usgs.gov/pub/imswelcom/). Anyone may

request existing data (Yamaguchi et al., 1998).

   For this project, the EOS database was searched for many volcanoes with crater

lakes that had been active during the life of ASTER and for which ground observations

were known to exist. Based on the availability of images, I chose several volcanoes to

explore for this study, including Aoba, Awu, Copahué, Ijen, Kelimutu, Kelut, Kusatsu-

Shirane, Poas, and Ruapehu volcanoes. When ASTER level 1B images had already been

produced for a certain date, I was able to request the AST04 Brightness Temperature at

Sensor product through the ASTER On-Demand Data Gateway (http://edcdaac.usgs.gov/

asterondemand/index.asp). If level 1B processing had not yet been completed for an

image, it was necessary to have a 1B product made before an AST04 image could be

obtained.

3.3 Calculating Water Temperatures from ASTER Images

3.3.1 Principles of Temperature Calculation Using TIR Data

   The surface of a crater lake emits TIR radiation as a function of its temperature

and emissivity (between 0.96 – 0.99 for water) (Salisbury and D'Aria, 1992). Planck's

function relates the amount of radiation emitted by an object to its temperature:

$$(3) \quad L(\lambda, T) = \varepsilon(\lambda) \frac{c_1}{\lambda^5 \pi (e^{\frac{c_2}{\lambda T}} - 1)}$$

where L is radiance, λ is wavelength, T is temperature, ε is emissivity, and c_1 and c_2 are constants (Oppenheimer 1993; Dash et al., 2002).

A portion of the radiance leaving the surface is absorbed by gases in the atmosphere, especially water vapor. The atmosphere also emits energy in the TIR and contributes up-welling radiance to the satellite as well as down-welling sky radiance to the ground. Transmissivity controls how much of the emitted radiance will reach the satellite rather than be attenuated by the atmosphere. The radiative transfer equation relates these terms as follows:

$$(4) \quad L_i^{sat} = \varepsilon_i \tau_i B_i(T_s) + L_i^{up} + (1 - \varepsilon_i)\tau_i L_i^{down}$$

where i is the band, ε is emissivity, and τ is transmissivity. The at-satellite radiance (L_i^{sat}) is equal to the sum of the radiance emitted from the surface (the first term, where B(T) indicates the radiance emitted from a perfect blackbody at temperature T), the upwelling path radiance (the second term), and reflected downwelling sky radiance (the third term) (Oppenheimer, 1993; Dash et al., 2002).

If atmospheric effects are removed, and we assume an emissivity of 1, temperature may be calculated by using the inverse of Planck's function:

$$(5) \quad T = \frac{c_2}{\lambda \ln\left[\dfrac{c_1}{\lambda^5 \pi L} + 1\right]}$$

(Oppenheimer, 1993; Dash et al., 2002).

3.3.2 The Split-Window Algorithm

In order to remove atmospheric effects and calculate reliable temperatures, a split-window algorithm was applied to the image data. Split-window methods were first developed to determine sea-surface temperatures (SST) from satellite data (see Njoku, 1990 for a review of SST split-window techniques). These techniques exploit the differential atmospheric absorption between two or more sensor bands at different wavelengths, assuming that the amount of attenuation is proportional to the difference in radiance measured in the two bands. It is essentially an empirical approach (McMillin, 1975; Njoku, 1990; Dash et al., 2002).

The radiative transfer equation can be rewritten for use in the split-window method as follows:

$$(6)\quad L(13) = B(13, T_{B13}) = \tau_0(13)B(13, T_s) + B(13, T_A)[1 - \tau_0(13)]$$

$$(7)\quad L(14) = B(14, T_{B14}) = \tau_0(14)B(14, T_s) + B(14, T_A)[1 - \tau_0(14)]$$

where B13 and B14 are the ASTER bands used in the algorithm and T_A is the average temperature of the atmosphere. If the difference in the amount of radiation reaching the satellite is due to differential absorption in the atmosphere, the above equations can be further simplified by combining with Planck's equation to yield this simple formula:

$$(8)\quad T_s = T_{13} + a(T_{13} - T_{14}) + b$$

and the coefficients a and b are determined by a linear regression of brightness temperature data versus in situ temperature measurements (McMillin, 1975; Njoku, 1990; Dash et al., 2002).

A. Bernard (pers. commun. 2004) developed a split-window algorithm for determining water temperatures of volcanic crater lakes using data from Taal volcano in the Philippines:

$$(9) \quad T_s = 0.050900273(B_{13}) - 0.040517907(B_{14}) + 0.897764116$$

This will be referred to as "the algorithm" or "the split-window algorithm" in this paper.

3.3.3 Temperature Calculation

In the typical case, 3 pixels were chosen from the center of each lake, representing the warmest pixels of lake water, and the results were averaged. However, in the case of the small lakes of Copahué, and Kusatsu-Shirane, only the "hottest" pixel was selected for each lake (Figure 3.2). By choosing the warmest pixels from the center of the lake, mixed pixels containing both water and land surface were avoided.

A necessary first step in calculating water temperatures from ASTER TIR images is a recalibration of the data. Tonooka et al. (2004) explained how the sensors of the ASTER instrument have been degrading since its launch and provided instructions for user-based recalibration, along with a web-accessible database where coefficients to be used in the calibration can be found. Because the recalibration is intended to be applied to the DN of a pixel of level 1B data, corresponding radiance values had to be calculated for brightness temperature data from the AST04 images used in this study. AST04 data is presented in degrees Celsius, with a scaling factor of 100. So, each value was divided by 100, and then the radiance was calculated using equation 3., Planck's function (Alley

and Jentoft-Nilsen, 1999). Then, the recalibration coefficients were applied (Abrams and Hook 2002).

After recalibration, the inverse of Planck's function (equation 5) was used to return the data to temperature values. Finally, the split-window algorithm was applied. For the larger lakes, where data from three pixels were used, the split-window results were averaged.

3.3.4 Comparison to Ground Truth

Once surface temperature has been determined from a satellite image, questions still remain as to the validity of the surface temperature as a true representation of the overall temperature of a lake. Fieldwork was undertaken at Lake Yugama on Kusatsu-Shirane volcano in order to explore the relationship between the radiant temperature of a lake surface, the actual surface temperature, and the overall water temperature of an example lake.

Radiant temperature measurements of the lake's surface waters were made during the fieldwork to demonstrate how temperatures calculated from radiance compare to the kinetic surface temperature. A temperature-depth profiler (CTD) was employed to give information about how the surface temperature relates to the temperature at depth, and data were taken at three different locations in the lake to check for lateral variability.

Table 3.1 Characteristics of the ASTER TIR subsystem (Yamaguchi et al., 1998).

Wavelength Region	Band Number	Spectral Range (μm)	Spatial Resolution
TIR	10	8.125 – 8.475	90 m
	11	8.475 – 8.825	
	12	8.895 – 9.275	
	13	10.25 – 10.95	
	14	10.95 – 11.65	

ASTER Data Processing System for TIR data

Science Data, Supplemental Instrument Data, and Spacecraft Ancillary Data

Image Data, Auxiliary Data, Radiometric Coefficients, and Geolocation Data

Radiometrically Calibrated and Geometrically Registered Radiance at Sensor

Brightness Temperature
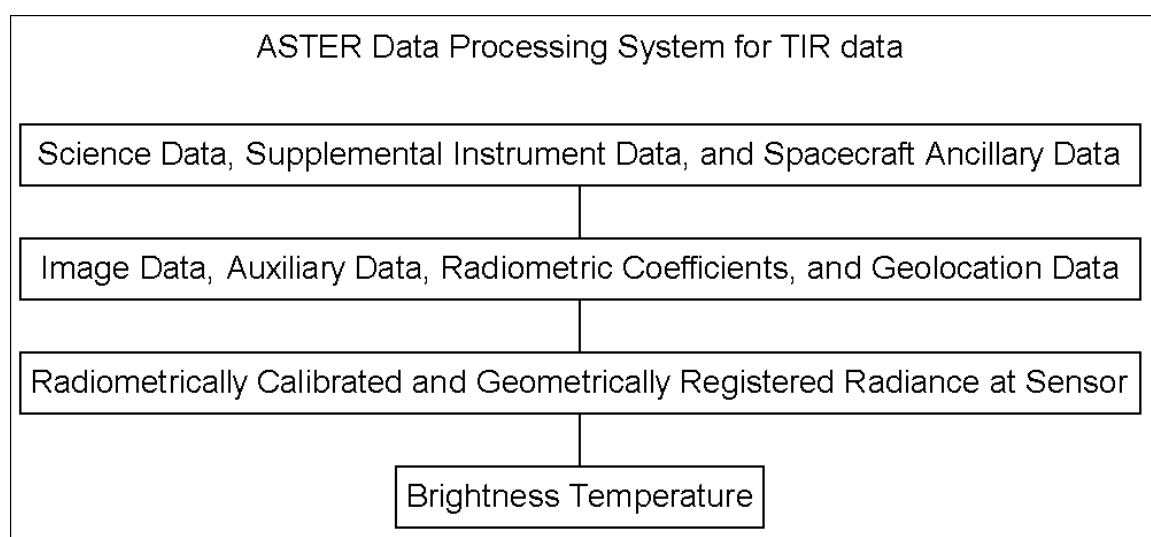
Figure 3.1 Flow chart illustrating the procedure for ASTER data processing
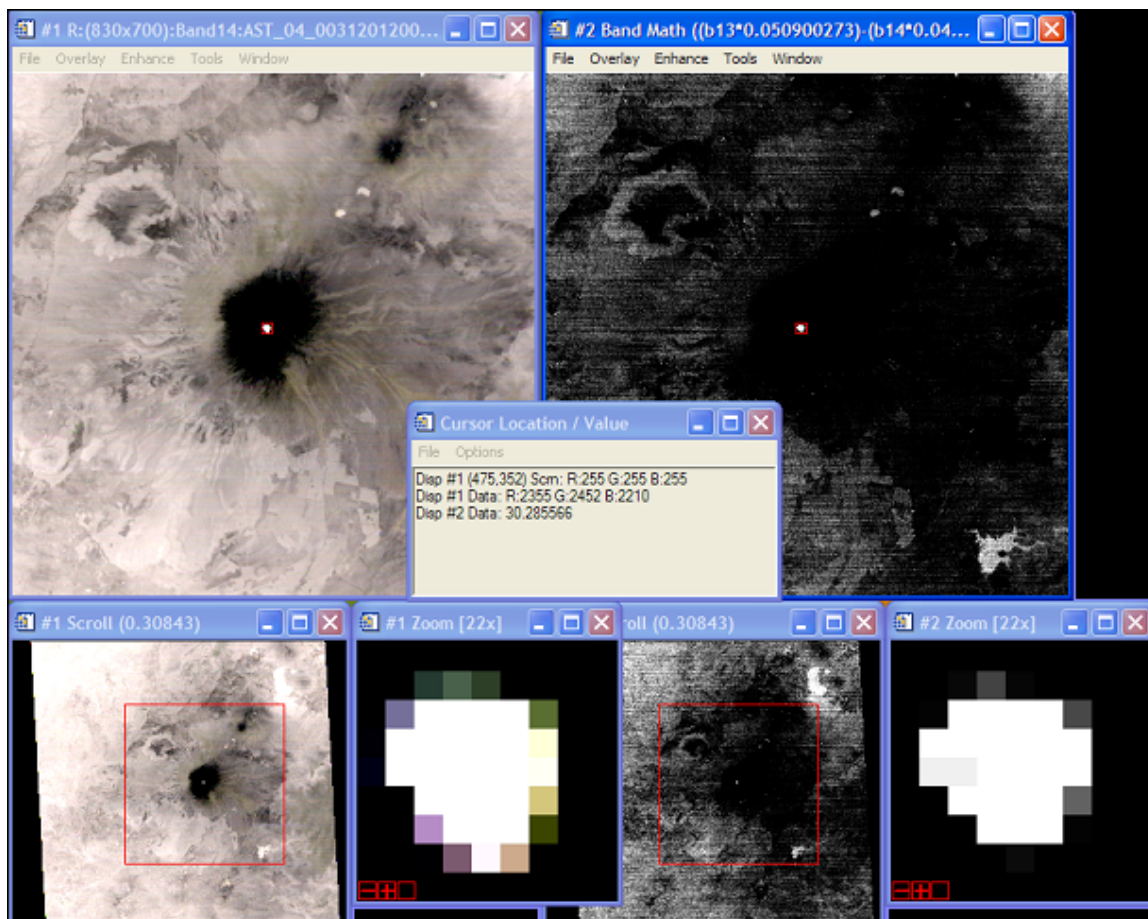
Figure 3.2 Selection of an appropriate lake water pixel

4. Validation of Method

4.1 Kusatsu-Shirane (2000-2005)

Japan's Kusatsu-Shirane volcano was selected to test the reliability of the split-window algorithm because of the wealth of ground-based temperature measurements, which are available for Lake Yugama, its crater lake. Also, I was able to carry out fieldwork at Lake Yugama during the summer of 2004, as discussed earlier. Kusatsu-Shirane is a stratovolcano on the island of Honshu located at 36.62 ºN and 138.54 ºE in a temperate climate. The summit elevation is approximately 2,100m. These characteristics mean that the lake exists under much different conditions than that of Taal volcano, which lies at low latitude in the Philippines and the relatively low elevation of 400m. Kusatsu-Shirane volcano last erupted in 1989, and in a state of repose throughout the study period (Siebert and Simkin, 2002).

The temperatures calculated using the split-window algorithm for Lake Yugama were compared to ground data recorded by the Kusatsu-Shirane Volcano Observatory (KSVO) for the period 2000-2005. Table 4.1 lists the granule ID, date, time, and center point for each of the 25 images used in the study, along with the AST04 temperature for the pixel selected to represent the lake, the temperature calculated using the split-window algorithm, and the average temperature measured from the ground for the corresponding date for images not entirely obscured by clouds. Figure 4.1 shows how each calculated split-window temperature compares to ground truth and figure y illustrates the improvement of the split-window algorithm, which uses a pixel-by-pixel adjustment for

atmospheric water, over the AST04 Brightness Temperature product, which does not

include an atmospheric correction. Overall, the agreement between the temperatures

calculated using the split-window method from ASTER images and ground truth is quite

good, typically ±1.5 ºC, with a maximum error of 6.3 ºC for cloud-free images. This is a

positive result, given that the split-window algorithm was developed under circumstances

that included a different atmospheric profile.

It should be noted that Lake Yugama, with an average diameter of just 280 m is

one of the smaller lakes studied, so temperatures were calculated using just one pixel,

rather than the average of 3 or 5 pixels. Because of this, the possibility of mixed pixels,

or those that include a percentage of dry land rather than just purely being composed of

lake water, is high. I believe that for larger lakes, the calculated temperatures should

have higher accuracy. In any case, the improvement of the split-window method over the

Brightness Temperature (calculated with no atmospheric correction) as seen in figure 4.2

is clear.

4.2 Summer 2004 Field Campaign

Fieldwork at Lake Yugama (Kusatsu-Shirane volcano) explored the temperature

distribution within a representative crater lake and also the variability of radiant

temperature measurements, taking into account environmental factors such as wind.

First, little variability was seen between surface temperatures measured at different

locations in the lake. However, CTD measurements of the water temperature at depth

revealed that, as expected, the overall temperature of the lake was somewhat different

from the surface temperature (figures 4.3, 4.4).

When the radiant temperatures taken at the surface of Lake Yugama are compared

to the bulk surface temperatures measured at less than 0.05 m with the CTD, the results

vary due to the skin effect (table 4.2). Wind speeds were low during the fieldwork

(average 0.8 m/s, maximum 2.7 m/s), so most of the surface cooling can probably be

attributed to evaporative heat loss at the air-water interface. Measurements were made

under partly cloudy conditions, so the higher skin temperature seen in some cases may be

attributed to downwelling radiation from clouds. Finally, in some locations on Lake

Yugama, sulfur particles suspended in the water might help to account for the apparently

lower radiant temperatures, because of the lower emissivity of the sulfur. Overall, the

daytime skin effect observed at Lake Yugama ranged from –0.88 to 0.68 ºC, with a mean

ΔT_{b-s} of 0.15 ºC (Table x).

4.2 Estimation of Error

There are multiple sources of error associated with results from the split-window

algorithm. These can be divided into three categories: instrumental error, application

error, and environmental error. The first of these derives from imprecision in the data

collected by ASTER, which has a theoretical NEΔT of 0.3 ºC. Changing the input data

by ± 0.3 ºC results in an imprecision of ± 1.9 ºC for the split-window algorithm results.

What I call application error arises from the fact that the algorithm was developed

under one set of climatic conditions, at Taal volcano, and, in this study, is being applied

outside of the region for which it was calculated. Atmospheric conditions change from one location to the next, with more or less water vapor in the atmosphere depending on the elevation and local climate, causing inaccuracy in the results. Fortunately, inaccuracies caused by these variations from one volcano to the next are systematic. So, while data from one crater lake may not be accurate with respect to that from a second lake, data from one lake should at least be accurate relative to other data from that same lake, allowing reliable thermal time series to be charted. Split-window results for Kusatsu-Shirane, when checked against in-situ temperature measurements, showed an average inaccuracy of $\pm$ 1.5 ℃

Finally, various environmental factors may influence the reliability of remotely sensed temperature data. As discussed earlier, the skin effect, which is dependent on wind speed, ambient air temperature, and solar heating, causes radiant surface temperatures to differ from bulk surface temperatures, introducing inaccuracy on the order of $\pm$ 1.5 ℃. Other environmental factors that may cause satellite-based temperature measurements to differ from temperatures measured at the ground arise from differences in the measurement methods. Local conditions may change between the times when ground- and satellite-based data are collected, even on the same day. Weather conditions such as rain or snowstorms might have an immediate, short-lived effect on the surface temperature. Or, diurnal variations might occur, for example if an increase in the amount of cold meltwater entering the lake during the day causes the surface to be cooler for a time. In general, environmental errors are hard to predict, and may be on the order of several degrees under the worst conditions (Oppenheimer, 1993).

Assumptions about error for the split-window algorithm results were made by

taking these three possible sources of error into account and considering how the

algorithm appeared to perform at Kusatsu-Shirane volcano. I assume an average

inaccuracy of $\pm$ 1.5 ºC for my data, with a precision of $\pm$ 1.9 ºC, keeping in mind that it is

possible for larger errors to exist under the most unfortunate environmental

circumstances.

Table 4.1 Images of Lake Yugama used, temperature of the lake pixel taken from the AST04 product for each, the temperature calculated using the split-window method (SW Temp), and corresponding ground-based temperature data (Ground Temp).

Granule ID	Date	Local Time	Center Point (Lat, Lon)	AST04 Temp (ºC) Band 14	Band 13	SW Temp (ºC)	Ground Temp (ºC)
SC:AST_L1B.003:2012504260	23-May-00	1:54:30 AM	36.81, 138.82	12.77	13.02	15.5	15.6
SC:AST_L1B.003:2003675190	30-May-00	2:00:47 AM	36.64, 138.41	17.33	17.19	18.3	17.3
SC:AST_L1B.003:2026658726	24-Dec-00	1:01:16 PM	36.76, 138.75	-1.15	0.11	6.2	6.2
SC:AST_L1B.003:2017822532	21-Mar-01	1:05:16 PM	36.41, 138.60	-0.26	0.21	3.0	4.3
SC:AST_L1B.003:2024698327	30-Mar-01	12:59:07 PM	36.77, 138.81	-6.88	-3.94	8.8	6.9
SC:AST_L1B.003:2018239657	4-Jul-01	12:56:37 PM	36.77, 138.82	18.28	18.99	23.6	23.5
SC:AST_L1B.003:2018331161	29-Jul-01	1:47:14 AM	36.84, 138.65	20.13	21.07	26.8	26.9
SC:AST_L1B.003:2004245962	5-Aug-01	1:53:18 AM	36.66, 138.26	22.00	22.29	25.4	25.0
SC:AST_L1B.003:2020240300	17-Mar-02	1:46:44 AM	36.64, 138.44	1.88	2.39	5.5	6.0
SC:AST_L1B.003:2006514890	9-Apr-02	12:55:49 PM	36.45, 138.95	4.51	4.18	3.8	9.8
SC:AST_L1B.003:2027032088	18-Apr-02	12:50:02 PM	36.70, 138.36	7.28	7.81	11.2	11.8
SC:AST_L1B.003:2007258759	5-Jun-02	1:47:09 AM	36.65, 138.36	15.86	16.09	18.5	18.3
SC:AST_L1B.003:2028966245	23-Jul-02	1:47:06 AM	36.65, 138.36	15.05	16.39	23.5	24.0
SC:AST_L1A.003:2008158239	8-Aug-02	1:46:50 AM	36.64, 138.42	23.08	23.77	28.4	27.3
SC:AST_L1B.003:2008691160	2-Oct-02	12:55:48 PM	36.39, 138.51	15.34	16.01	20.3	21.0
SC:AST_L1B.003:2026658929	9-Jan-04	12:55:38 PM	36.43, 138.74	-1.80	-1.05	2.9	5.2
SC:AST_L1B.003:2021922732	13-Mar-04	12:54:59 PM	36.45, 138.90	-4.02	-2.64	3.8	4.5
SC:AST_L1B.003:2022681793	7-Apr-04	1:45:11 AM	36.62, 138.54	4.45	5.04	8.5	9.8
SC:AST_L1B.003:2028966268	3-Jun-04	1:39:12 AM	36.82, 138.78	14.45	15.23	19.9	19.6
SC:AST_L1B.003:2024977430	3-Jul-04	12:54:20 PM	36.40, 138.54	17.35	18.97	27.2	24.1
SC:AST_L1B.003:2025105219	19-Jul-04	12:54:21 PM	36.39, 138.51	10.22	11.79	19.6	24.2
SC:AST_L1B.003:2025988690	30-Sep-04	12:47:49 PM	36.69, 138.32	17.70	17.82	19.9	22.3
SC:AST_L1B.003:2026774535	10-Nov-04	1:38:02 AM	36.84, 138.61	8.83	8.87	10.2	16.5
SC:AST_L1B.003:2027720595	29-Jan-05	1:38:30 AM	36.87, 138.44	0.48	1.01	4.1	3.3
SC:AST_L1B.003:2028966281	9-Mar-05	1:44:43 AM	36.63, 138.49	1.06	1.41	3.8	3.8
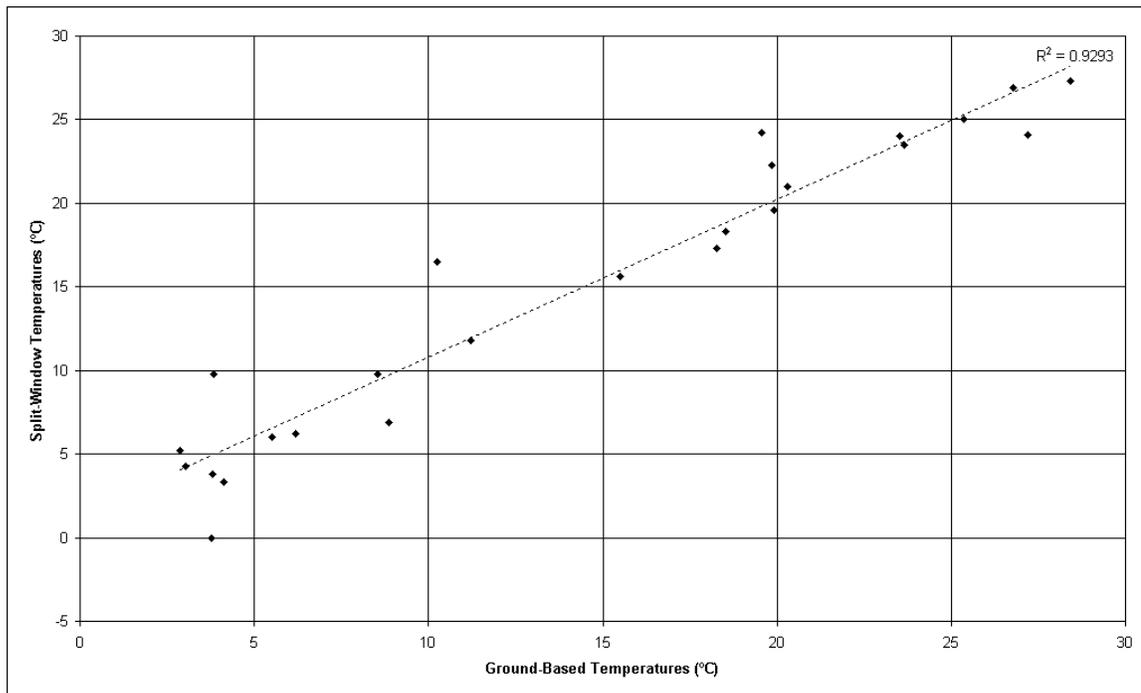
Figure 4.1 Comparison of Calculated Split-Window Temperatures to Ground Truth from Lake Yugama.
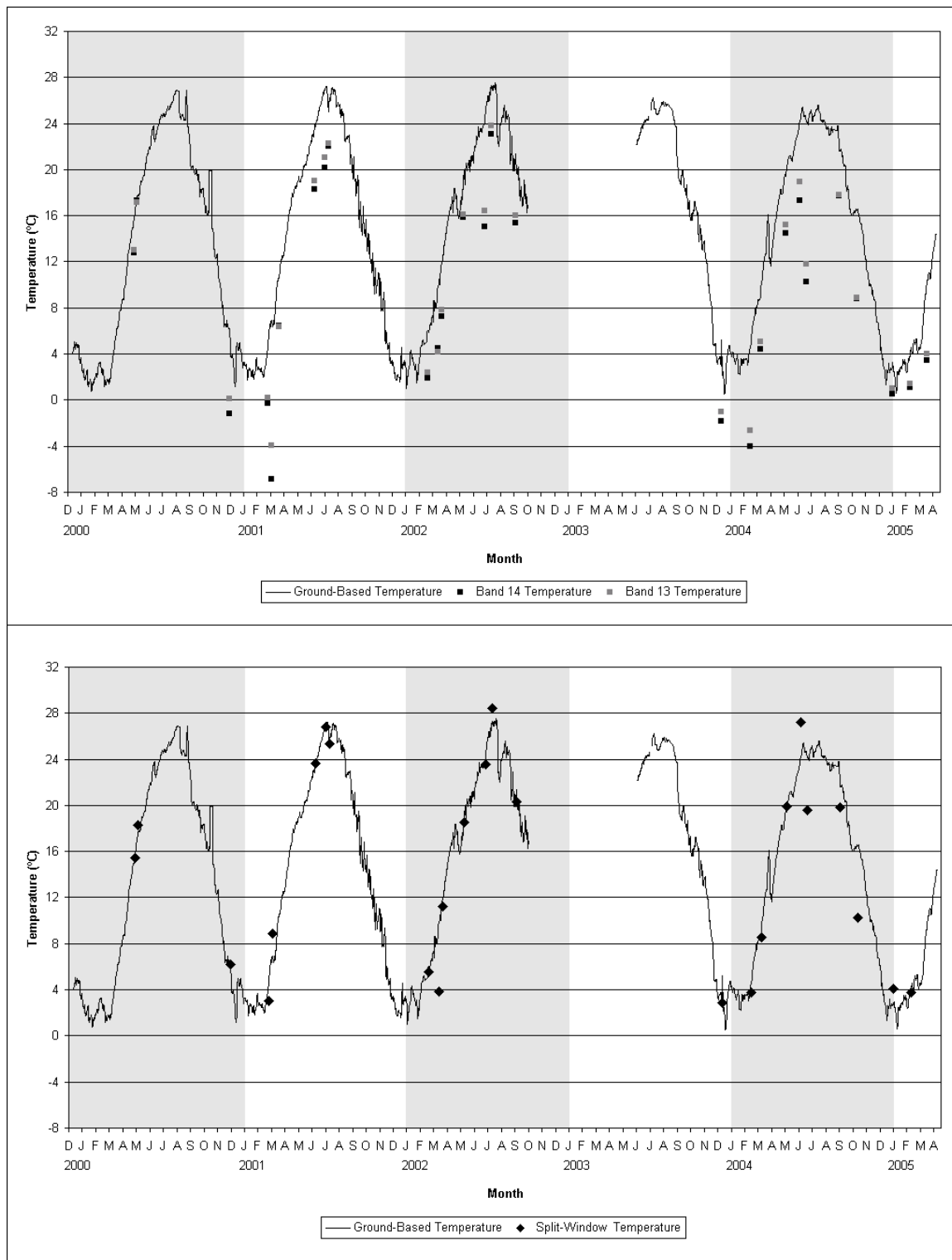
Figure 4.2 For the period 2000-2005, Lake Yugama Brightness Temperature for Bands 14 and 13 from the AST04 product compared to ground truth (top) and calculated split-window temperatures of Lake Yugama compared to ground truth (bottom).
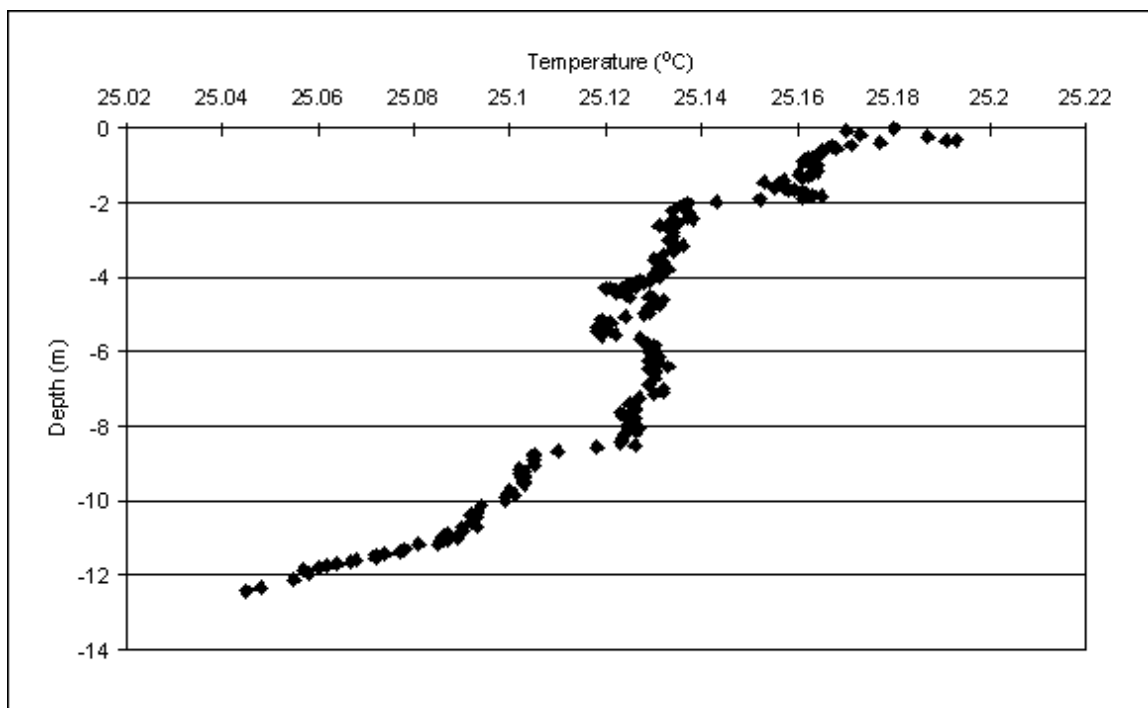
Figure 4.3 Temperature profile at Point A.
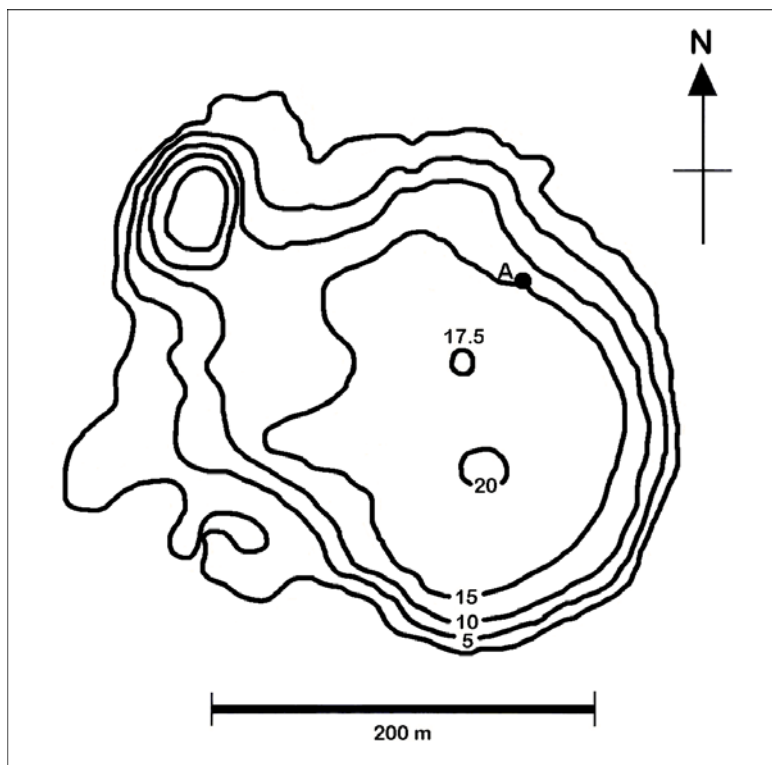
Figure 4.4 Map of Lake Yugama showing the approximate location of the CTD profile shown above. Depth contours in meters.

Table 4.2 Radiant Skin Temperature, Bulk Surface Temperature, and the Bulk-Skin
Temperature Deviation measured in Lake Yugama

Date	Approximate Local Time	Average Wind Speed (m/s)	Radiant Skin Temperature (°C)	Bulk Surface Temperature (°C)	ΔT_{b-s} (°C)
27 Jul 04	15:00	1.5	24.5	25.18	0.68
27 Jul 04	15:30	0.9	25.1	25.15	0.05
28 Jul 04	10:00	0.8	26.3	25.42	-0.88
28 Jul 04	10:15	0.4	24.5	25.18	0.68
28 Jul 04	10:30	0.5	25.0	25.24	0.24

5. Results and Discussion

5.1 Availability of ASTER Images

This project began with a thorough search of the ASTER image database. Volcanoes for this study were chosen based on how many usable images of the crater lake were available for analysis. Of the 18 volcanoes for which a search was conducted, 5 were selected as having adequate numbers of usable (not cloudy or otherwise unclear) images with which to construct a time-series of observations. For this study, both level 1A and level 1B images were easy to acquire. Note however, that independent researchers undertaking future studies who wish to acquire images for free through the ASTER On-Demand website are limited to those for which 1B processing has already been completed. Fewer images meet this criterion. Table 5.1 summarizes the results of the image search. Taal's crater lake was excluded from consideration because it served as the site where A. Bernard (personal communication, 2005) developed the split-window algorithm. Of the remaining volcanoes, Copahué, Ijen, Kusatsu-Shirane, Poás, and Ruapehu had the greatest number of usable images (>20 in each case) and were selected as example cases.

5.2 Split-Window Temperature Records (2000-2005)

5.2.1 Thermal History of Ruapehu Volcano

New Zealand's Ruapehu volcano, located in the Taupo Volcanic Zone on the North Island at 39.28 °S and 175.57 °E, is a stratovolcano that contains a crater lake

named, aptly, Crater Lake (figure 5.1). Crater Lake, at an elevation of ~2,700 m, is
approximately 400 m in diameter and 600 m at its deepest point. All historical activity at
Ruapehu has originated from the Crater Lake vent, with the last major eruption having
taken place during September – October 1995. As with most volcanoes containing crater
lakes, lahars are a major hazard associated with the volcano. Also, the possibility of an
overflow and rapid erosion of ice or debris dams, is of increasing concern as the lake
level continues to rise (Houghton et al., 1987; Hurst and McGinty, 1999; Siebert and
Simkin, 2002; Institute of Geological and Nuclear Sciences, 2005).

Although no eruptive activity has occurred at Ruapehu since the launch of
ASTER in 1999, several heating cycles have occurred. The 25 ASTER images analyzed
using the split-window algorithm are listed in Table 5.2. Figure 5.2 shows the
temperature record for Crater Lake from 2000 – 2005, with results from both the split-
window algorithm and reported ground data. Starting in April of 2000, there was an
episode of moderate volcanic tremor, followed by a period of low seismic activity.
Similar episodes of tremor occurred frequently and they are charted on the temperature
graph of Ruapehu, with an indication of their relative strength. Volcanic earthquakes
sometimes occurred during this time period, and they are also noted on the graph. Steam
plumes occurred, the result of hydrothermal activity in the lake, or due to the right
combination of atmospheric conditions above the warm lake, and are also on the graph
(Smithsonian Institution, 2005a).

The most interesting time frame during the study period was late 2002 to early
2003. Starting the second week of September 2002, there were 4 short bursts of tremor,

followed by 5 more in October. Volcanic earthquakes occurred in November and the

temperature of Crater Lake rose 5 ℃ over this time. Lake temperatures continued to

climb through December, to a high of 40 ℃ in January. The activity slowed in February

2003 to background levels and Crater Lake's temperature dropped to 30 ℃ by the

beginning of March. From early March to mid-May, water temperature increased to 41.6

℃, activity that was again accompanied by an increased level of tremor and volcanic

earthquakes.

Results of the split-window algorithm provide a parallel record of the temperature

changes during this time period (figure 5.3). During times when field measurements

were not available, ASTER data is an excellent supplement. For example, although

between 26 November and 5 December 2002 ground-based temperature measurements

were not taken, we can see from the satellite image of 1 December that the water

temperature had continued to rise. If a severe increase in volcanic tremor or other

warning signs had been observed, the satellite data of 26 December 2002 and 18 January

2003 could have taken the place of dangerous field sampling. In this case, no eruptive

activity occurred, but it illustrates that ASTER split-window estimates of crater lake

temperatures correlate well with ground measurements, and can thus serve as a safe

substitute for field work that would be risky at such times of seismic and thermal unrest.

5.2.2 Thermal History of Poás Volcano

Poás is a complex stratovolcano, located at 10.20 ℃N and 84.23 ℃W in Central

Costa Rica. The summit region of Poás contains two crater lakes: Botos, a cold

freshwater lake, and Laguna Caliente, a hot acid lake in the active crater at around 2,300

m elevation (figure 5.4). Frequent phreatic and phreatomagmatic eruptions have

originated from this active crater in historic times, often including the ejection of water

from Laguna Caliente (Brantley et al., 1992; Siebert and Simkin, 2002).

Temperatures of Laguna Caliente depend not only on the thermal output of the

volcano, but also on rainfall, which is high in the region, at approximately 3.5 m per year

(with the dry season being from January – May). The last major activity at Poás occurred

in 1952-53 and included the loss of Laguna Caliente. The lake reappeared in 1967 and

since that time and, prior to 1990, lake water temperatures tended to range from 40 – 60

ºC, although temperatures as high as 96 ºC were observed during the active period of

1986-89, discussed earlier. Most recently, there were eruptive events during April –

September 1994 and August 1995 – January 1996 (Brown et al., 1989; Brown et al.,

1991; Martínez et al., 2000; Smithsonian Institution, 2005b).

When ASTER was launched in December of 1999, Poás was in the midst of a

period of elevated seismicity that lasted through June of 2000. This activity was

accompanied by bubbling in the crater lake, which reached a maximum temperature of 41

ºC in March of 2000. Seismicity increased further in May of 2000 and new fumaroles

appeared in the crater. Seismicity had decreased by July and between July 2000 and

August of 2004, the lake level and temperature fluctuated between 21 – 40 ºC with no

other signs of eruptive activity. Seismic activity stayed relatively stable, except for a

small increase in early September 2002, which coincided with the highest recorded

temperature of Laguna Caliente during this period, 41.5 ºC (Smithsonian Institution, 2005b).

Table 5.3 shows the 9 images analyzed using the split-window technique. The results of the split-window algorithm are charted, along with ground-based temperature measurements, in figure 5.5. Split-window results follow the temperature trends well as Laguna Caliente warms and cools twice during the period when ASTER images were available. As is expected, split-window results with the highest error are those for which the images were partly cloudy, and the lake is partially masked by clouds which block the transmission of radiation and make the lake appear colder than it really was.

5.2.3 Thermal History of Kawah Ijen Volcano

Kawah Ijen volcano, in eastern Java, Indonesia (8.06 ºS, 114.24 ºE), contains a large crater lake, approximately 700 m in diameter and 200 m deep, at around 2,300 m elevation (figure 5.6). Kawah Ijen has been frequently active in historic times, including throughout the 2000-2005 period for which ASTER images are available (Siebert and Simkin, 2002).

During the 1990s, numerous phreatic eruptions occurred from the crater lake of Kawah Ijen. Increased levels of seismicity and volcanic tremor, as well as temperature increases in the crater lake sometimes preceded these, although not in all cases. Another indicator of forthcoming activity at Kawah Ijen has been changes in the color of the crater lake. For example, a change from whitish-green to brown occurred before 3 phreatic eruptions in July of 1993 (Smithsonian Institution, 2005c).

The first sign of increased activity at Kawah Ijen since the launch of ASTER was an increase in the number of earthquakes in mid-June of 2000 and an increase in volcanic tremor, accompanied by a white ash plume which rose from the summit. After this first activity, seismicity increased still further, and another ash eruption took place in late August. Continuous tremor began in late September, but was discontinuous again by late October (Smithsonian Institution, 2005c).

The first usable ASTER image was from 6 October 2002, which showed a temperature of 31 ℃ (table 5.4). Split-window results indicated that the temperature of the crater lake rose between then and the end of 2001, which coincided with another period of increased seismicity and tremor that began in early 2001. Available earthquake and tremor data is charted in figure 5.7, along with ground-based temperature measurements of the crater lake, and results of the split-window algorithm for the 23 images analyzed of Kawah Ijen. Temperatures appear to have remained high through at least mid-2002, when plumes were again observed, reaching up to 100 m above the summit. This period of elevated seismicity continued through November of 2002, with plumes sometimes being observed then decreased in December of 2002 (Smithsonian Institution, 2005c).

Gas plumes and the onset of continuous tremor followed an increase in seismicity in October of 2003 that lasted through the end of the year. This was preceded by crater lake temperatures above 40 ℃ as seen in the ASTER images. Temperatures increased to the warmest observed for the study period in mid-2004, reaching a maximum of around 45 ℃. This final warming episode was synchronous with increased tremor, foaming and

color changes in the lake, and the ejection of sulfuric rocks from the crater. By early 2005, for which the last images were analyzed, activity had slowed and lake temperatures dropped once again below 40 ºC (Smithsonian Institution, 2005c).

5.2.4 Thermal History of Copahué Volcano

Argentina's Copahué stratovolcano is located at 38.85 ºS and 71.17 ºW, on the Chilean-Argentinean border, part of the Southern Andean Volcanic Zone (figure 5.8). The eastern, active crater contains the Del Agrio crater lake (~300 m diameter) at approximately 2,800 m elevation. This crater lake was ejected twice during eruptions in 1992 and 1995-96, along with liquid sulfur, which must be present in the lakebed. The lake was quickly reestablished after each eruption, fed by glacial meltwater and hydrothermal fluids. Temperatures of the crater lake range from 21 – 54 ºC, and the lake is generally well mixed, although it may become thermally stratified during the summer months (Varekamp et al., 2001; Naranjo and Polanco, 2004; Siebert and Simkin, 2002).

The most recent eruption of Copahué volcano, from July – October 2000 was the largest of historic times. Varekamp et al. (2001) reported from ground-based measurements that crater lake water temperatures increased prior to the eruption, from 21 ºC in January of 1999 to 33 ºC in November, but unfortunately, no ASTER images are available for analysis during this time period. The main precursor to the eruption of 1 July 2000 was an increase in Mg flux in the Upper Rio Agrio, the outflow from the Del Agrio crater lake, several weeks prior to the eruption, from a fresh magmatic source (Varekamp et al., 2001; Smithsonian Institution, 2005d).

Although no further eruptive activity occurred between the reestablishment of the crater lake in January of 2001 and early 2005, the 16 ASTER images analyzed during this time period (table 5.5) provide a record of crater lake temperatures that may be useful in interpreting future activity. According to the split-window results (figure 5.9), temperatures ranged from 34 ºC to 55.6 ºC over the study period.

In the future, satellite monitoring of water temperatures of the remote Del Agrio crater lake at Copahué, for which field access is difficult, may prove to be an invaluable tool. A population of up to 1,500 in the tourist destination of Caviahue would be threatened by future activity, which, according to Varekamp et al. (2001), is increasingly likely as the 2000 eruption heralded an awakening of the volcano.

5.3 Summary

In total, 64 images of the crater lakes of 4 volcanoes were analyzed using the split-window technique of this study. These volcanoes cover a wide range of geographical locations and climates, from Indonesia to temperate New Zealand, tropical Costa Rica and the Patagonian desert of Argentina, and occur at a variety of elevations, from 2,300 to 2,800 m. All are volcanoes that have erupted in historic times and continue to threaten nearby populations. For each volcano, a temperature record was established for the crater lake over the study period. In some cases, such as that of Ruapehu volcano, satellite observations alone would have sufficed to sketch temperature trends had ground-based temperature measurements not been available or if it was determined that field measurements were too dangerous to attempt during periods of increased activity. In the

case of Copahué volcano, the crater lake of which is difficult to access, temperature

measurements from ASTER images might provide the only observations of increased

water temperatures that might precede future eruptions. Overall, the split-window

method, which was developed using data from Taal volcano (elevation 400 m) in the

Philippines, performed well enough under these varied conditions to provide results that

are precise, if not necessarily accurate. In this way, results of the split-window algorithm

applied to ASTER imagery are reliable for establishing thermal trends for the crater lakes

of active volcanoes.

Table 5.1 Availability of ASTER images for volcanoes with crater lakes.

Volcano Name	Total Images	Total Usable Images	% Images Usable	Processed to 1B	Processed to 1B Usable	% Freely Available, Usable
Aoba	58	9	15.5	46	8	13.8
Awu	41	9	22.0	23	4	9.8
Copahué	57	30	52.6	35	15	26.3
Ebeko	89	13	14.6	74	10	11.2
Egon	29	11	37.9	27	13	44.8
El Chichón	41	7	17.1	19	3	7.3
Ijen	60	22	36.7	60	24	40.0
Inielika	39	4	10.3	39	4	10.3
Irazú	69	8	11.6	36	7	10.1
Kaba	43	5	11.6	26	3	7.0
Kelimutu	26	7	26.9	23	5	19.2
Kelut	28	6	21.4	24	5	17.9
Kusatsu-Shirane	86	31	36.0	50	23	26.7
Pinatubo	100	15	15.0	100	15	15.0
Poás	79	23	29.1	46	15	19.0
Rincón de la Vieja	68	8	11.8	44	7	10.3
Ruapehu	77	31	40.3	59	23	29.9
Taal	60	23	38.8	57	19	31.7
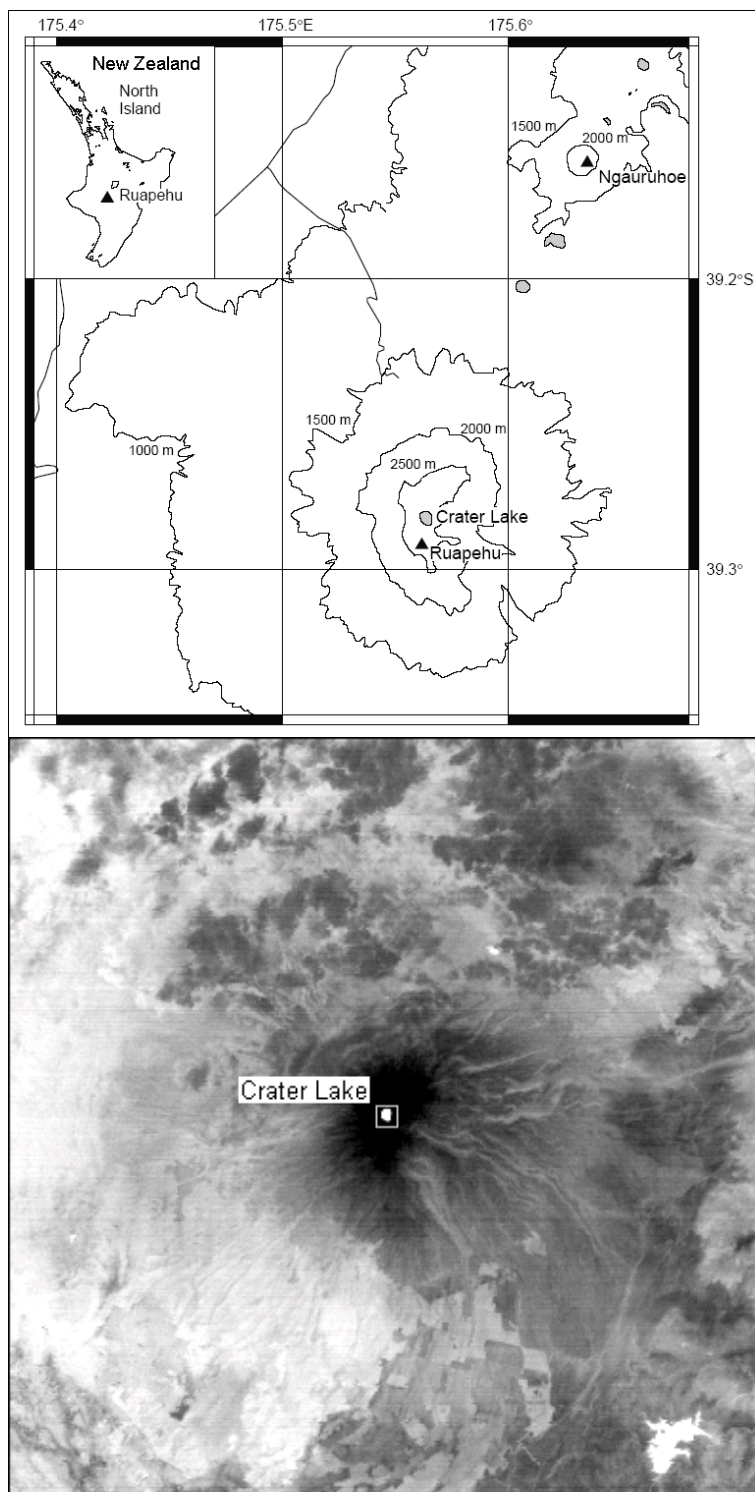
Figure 5.1 a) Map of Ruapehu showing the location of Crater Lake. Inset shows the location of Ruapehu on the North Island of New Zealand (Hurst, 1998). b) ASTER thermal image of Ruapehu volcano, with Crater Lake within the square.

Table 5.2 Images of Crater Lake on New Zealand's Ruapehu volcano, the average temperature of the three hottest lake pixels taken from the AST04 Brightness Temperature Product for each and the temperature calculated using the split-window method.

Granule ID	Date	Local Time	Center Point (Lat, Lon)	AST04 Temp (ºC) Band 14	AST04 Temp (ºC) Band 13	SW Temp (ºC)
SC:AST_L1B.003:2012489640	1-May-00	10:39:58 PM	-39.09, 175.96	48.5	48.8	52.6
SC:AST_L1B.003:2012502870	10-May-00	10:33:27 PM	-39.34, 175.38	23.8	27.3	40.1
SC:AST_L1B.003:2017368663	12-Jan-01	10:35:57 PM	-39.06, 175.71	25.5	26.2	32.2
SC:AST_L1B.003:2017890294	11-Apr-01	11:23:35 AM	-39.53, 175.46	26.9	27.6	32.3
SC:AST_L1B.003:2018306552	23-Jul-01	11:27:33 AM	-39.30, 175.43	15.4	16.4	22.2
SC:AST_L1B.003:2018433219	26-Aug-01	11:14:33 AM	-39.13, 175.86	13.7	14.8	20.5
SC:AST_L1B.003:2018544413	25-Sep-01	11:25:30 AM	-39.29, 175.48	16.4	17.3	23.3
SC:AST_L1B.003:2018737113	5-Nov-01	10:22:26 PM	-39.35, 175.45	17.2	18.0	22.3
SC:AST_L1B.003:2027640799	9-Feb-02	11:15:02 AM	-39.52, 175.49	27.9	29.0	37.1
SC:AST_L1B.003:2006286241	13-Mar-02	11:14:34 AM	-39.52, 175.50	24.9	26.1	32.9
SC:AST_L1B.003:2007878072	14-Apr-02	11:14:38 AM	-39.52, 175.51	23.2	24.2	29.5
SC:AST_L1B.003:2026199052	4-Aug-02	11:14:50 AM	-39.53, 175.45	15.0	16.1	22.4
SC:AST_L1B.003:2008895026	23-Oct-02	11:14:25 AM	-39.52, 175.47	14.7	15.4	20.3
SC:AST_L1B.003:2010721686	1-Dec-02	11:20:52 AM	-39.29, 175.50	23.4	24.7	30.4
SC:AST_L1B.003:2022360216	26-Dec-02	10:19:05 PM	-39.40, 175.76	33.5	35.0	41.4
SC:AST_L1B.003:2010869774	18-Jan-03	11:20:30 AM	-39.28, 175.57	33.4	34.2	40.8
SC:AST_L1B.003:2013179895	16-Mar-03	11:14:00 AM	-39.50, 175.66	27.7	29.0	36.9
SC:AST_L1B.003:2025311925	1-Apr-03	10:18:35 PM	-39.34, 175.39	25.3	28.2	41.5
SC:AST_L1B.003:2012754426	8-Apr-03	11:20:10 AM	-39.28, 175.53	30.8	32.3	39.2
SC:AST_L1B.003:2030001340	24-Apr-03	10:24:10 PM	-39.00, 175.30	32.9	34.0	40.7
SC:AST_L1B.003:2015244028	6-Jul-03	11:13:02 AM	-39.47, 175.87	15.2	16.9	27.4
SC:AST_L1B.003:2015318836	13-Jul-03	11:18:58 AM	-39.34, 175.19	17.7	18.8	25.3
SC:AST_L1B.003:2018714226	18-Nov-03	11:20:10 AM	-39.30, 175.46	12.9	13.6	18.4
SC:AST_L1B.003:2030001345	4-Dec-03	10:24:55 PM	-39.08, 175.86	16.4	17.0	21.2
SC:AST_L1B.003:2022029885	18-Mar-04	11:13:36 AM	-39.52, 175.48	24.9	26.0	32.8
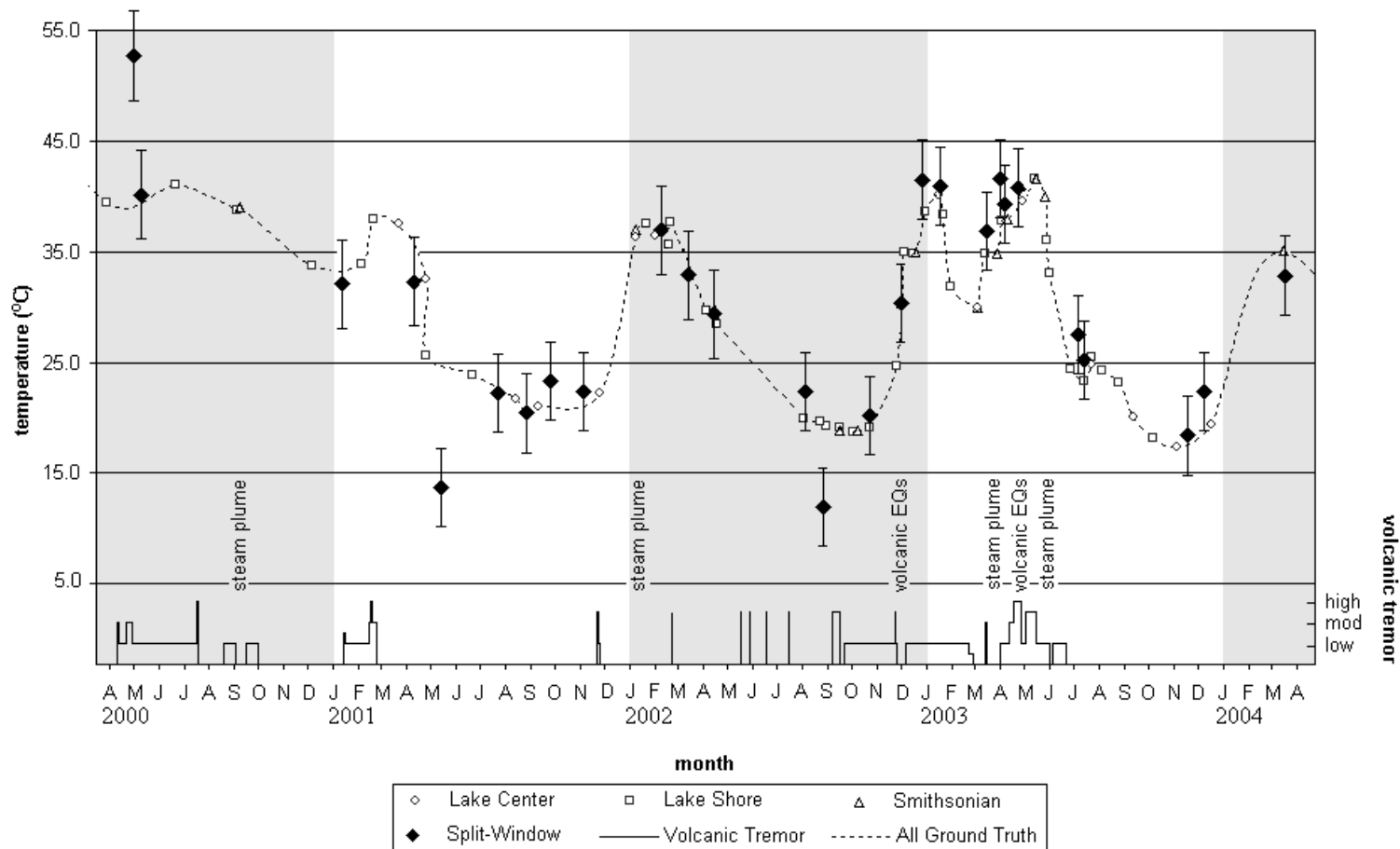
Figure 5.2 Temperatures calculated using the split-window algorithm versus reported ground-based results during the time period 2000-2004. Volcanic tremor is charted at the bottom, when reported, as low, moderate, or high. Also noted are volcanic earthquakes and steam plumes. Lake Shore and Lake Center data courtesy of B. Scott (pers. commun., 2005), other ground data, volcanic tremor, volcanic earthquake, and steam plume information (Smithsonian Institution, 2005a).
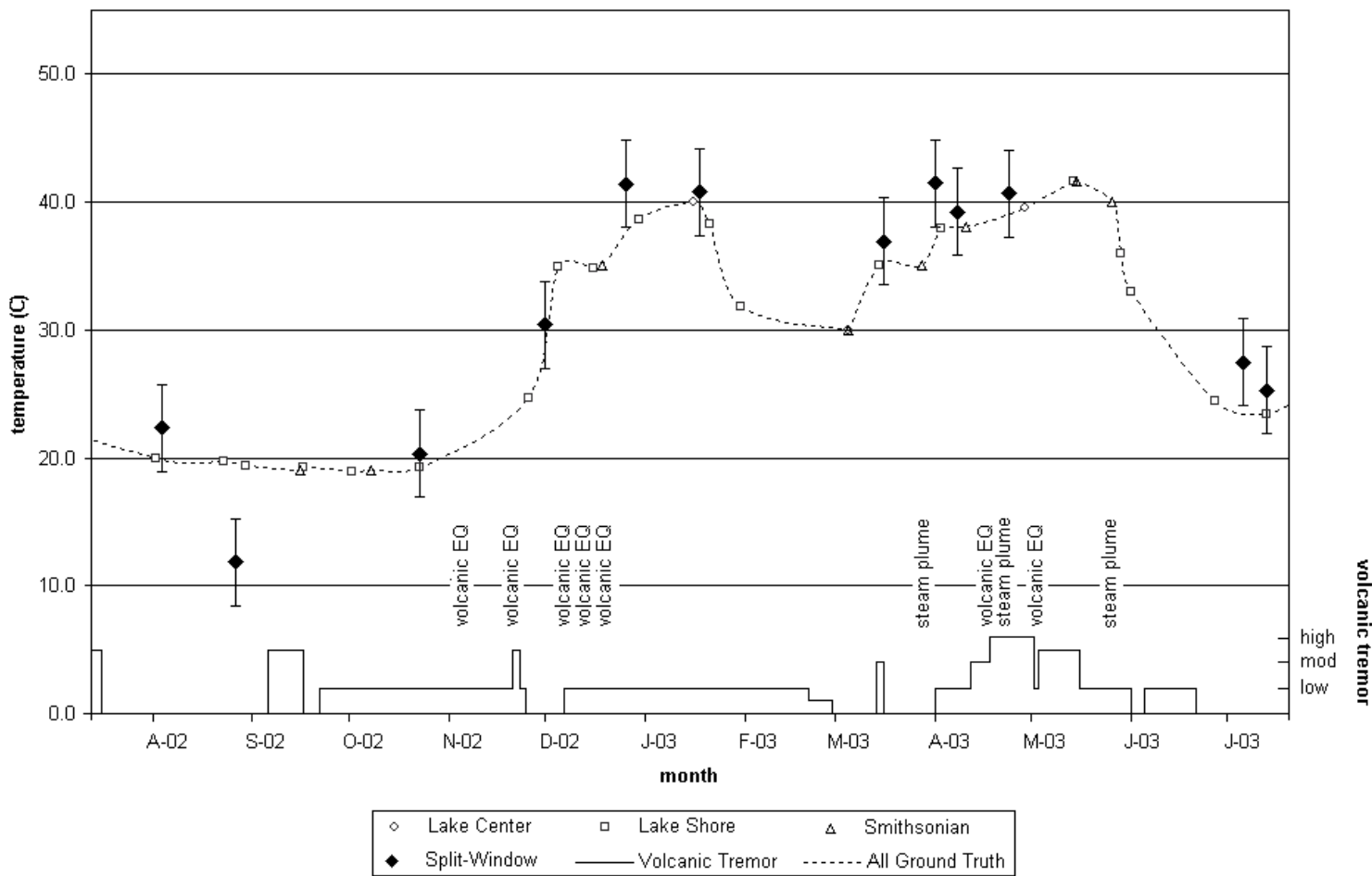
Figure 5.3 Thermal history of Ruapehu Crater Lake from July 2002 – July 2003. Split-window algorithm results are shown as closed diamonds. Lake Shore and Lake Center data, B. Scott (pers. commun., 2005), other ground data, volcanic tremor, volcanic earthquake, and steam plume information (Smithsonian Institution, 2005a).
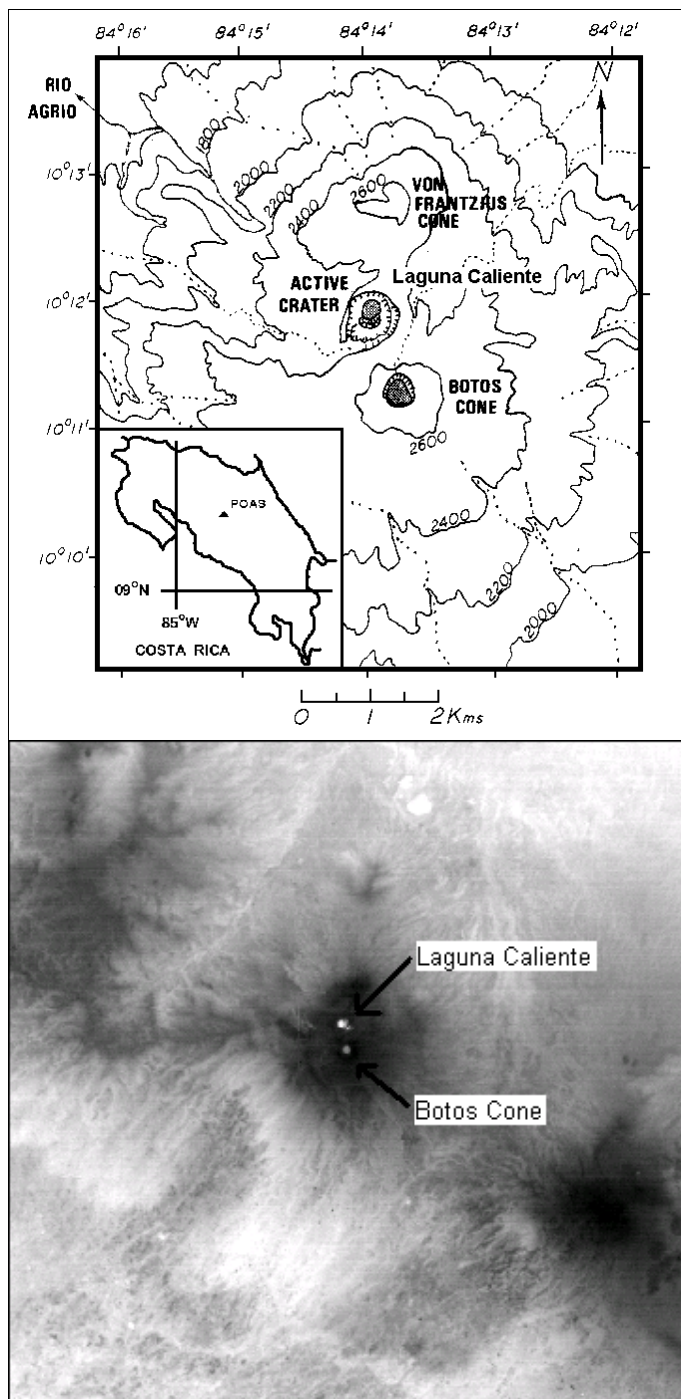
Figure 5.4 a) Map showing the main features of Poás volcano, including the hot crater lake, Laguna Caliente (Rowe et al., 1992). Inset shows the location of Poás within central Costa Rica (Casertano et al., 1987). b) Thermal ASTER image of Poás, with both summit lakes visible. The warmer Laguna Caliente appears lighter on the thermal image. North is toward the top in this image.

Table 5.3 Images of Laguna Caliente on Costa Rica's Poás volcano, the average temperature of the three hottest lake pixels taken from the AST04 Brightness Temperature Product for each and the temperature calculated using the split-window method. The notation "sl. cl." in the notes column indicates images where the crater lake may have been partially obscured by clouds.

Granule ID	Date	Local Time	Center Point (Lat, Lon)	AST04 Temp (ºC) Band 14	AST04 Temp (ºC) Band 13	SW Temp (ºC)	Notes
SC:AST_L1B.003:2017587700	7-Feb-01	4:07:52 AM	10.02, -84.01	20.5	22.0	29.7	
SC:AST_L1B.003:2018611368	12-Oct-01	4:07:46 AM	10.20, -84.31	17.0	18.2	24.2	sl. cl.
SC:AST_L1B.003:2027537875	25-Jan-02	3:58:21 AM	10.02, -84.00	15.6	16.4	21.1	sl. cl.
SC:AST_L1B.003:2010717200	18-Dec-02	4:03:31 AM	10.20, -84.33	23.1	25.2	35.5	sl. cl.
SC:AST_L1A.003:2012434842	24-Mar-03	4:02:49 AM	10.24, -84.08	23.6	26.3	38.3	
SC:AST_L1B.003:2018715248	19-Nov-03	4:02:46 AM	10.20, -84.36	19.9	21.0	26.7	
SC:AST_L1B.003:2030001346	31-Jan-04	4:12:31 PM	10.19, -84.21	19.5	19.9	23.2	
SC:AST_L1B.003:2022345445	26-Mar-04	4:02:11 AM	10.22, -84.19	17.7	18.0	20.5	
SC:AST_L1B.003:2025161381	25-Jul-04	3:55:36 AM	10.03, -83.98	15.2	16.4	22.4	sl. cl.
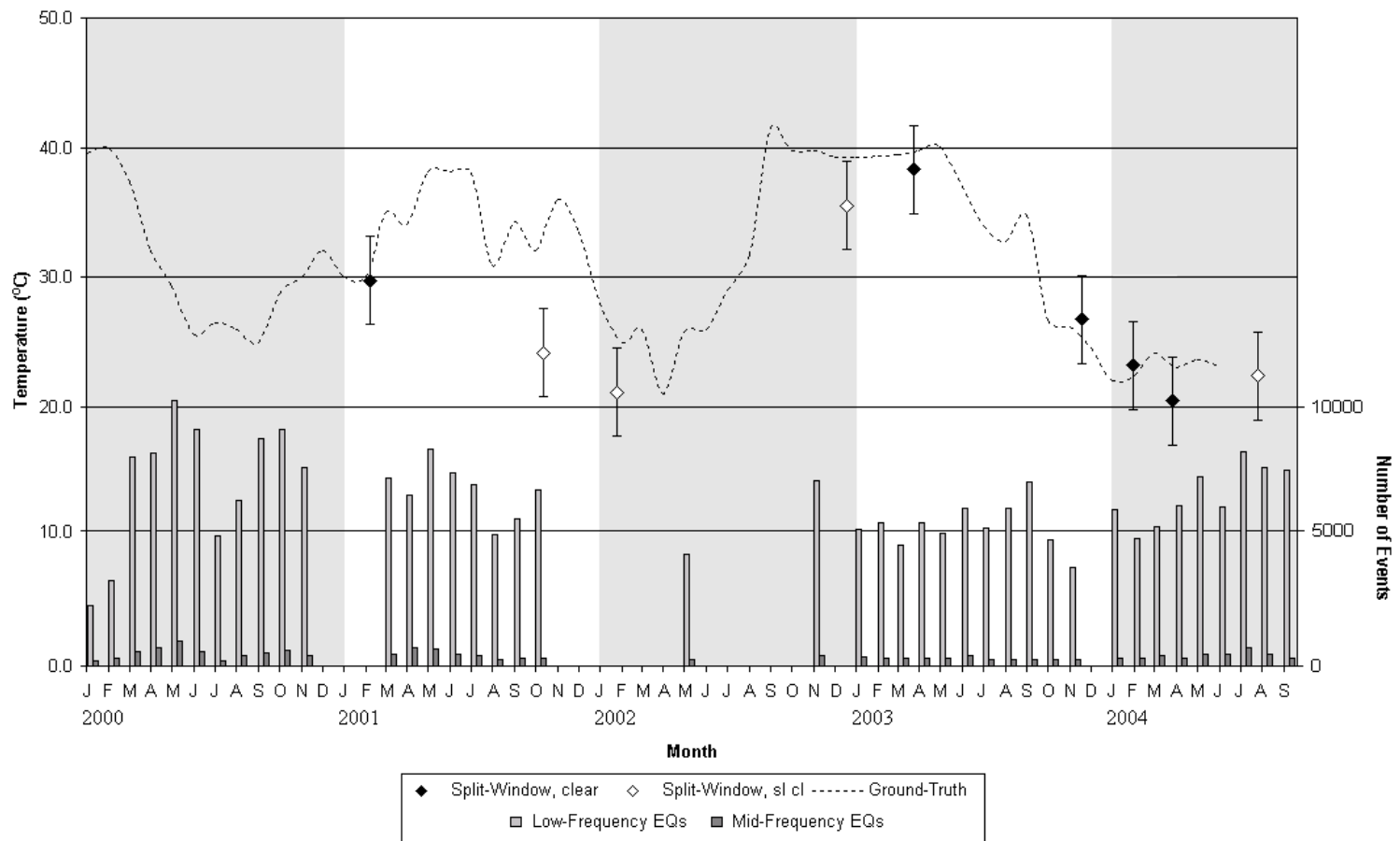
Table 5.5 Thermal history of Laguna Caliente from Jan. 2000 – Aug. 2004. Split-window algorithm results are shown as closed diamonds for clear images and open diamonds for partly cloudy images. Ground data courtesy of R. Mora (pers. commun., 2005), earthquake data from reports published by OVSICORI-UNA (http://www.una.ac.cr/ovsi/).
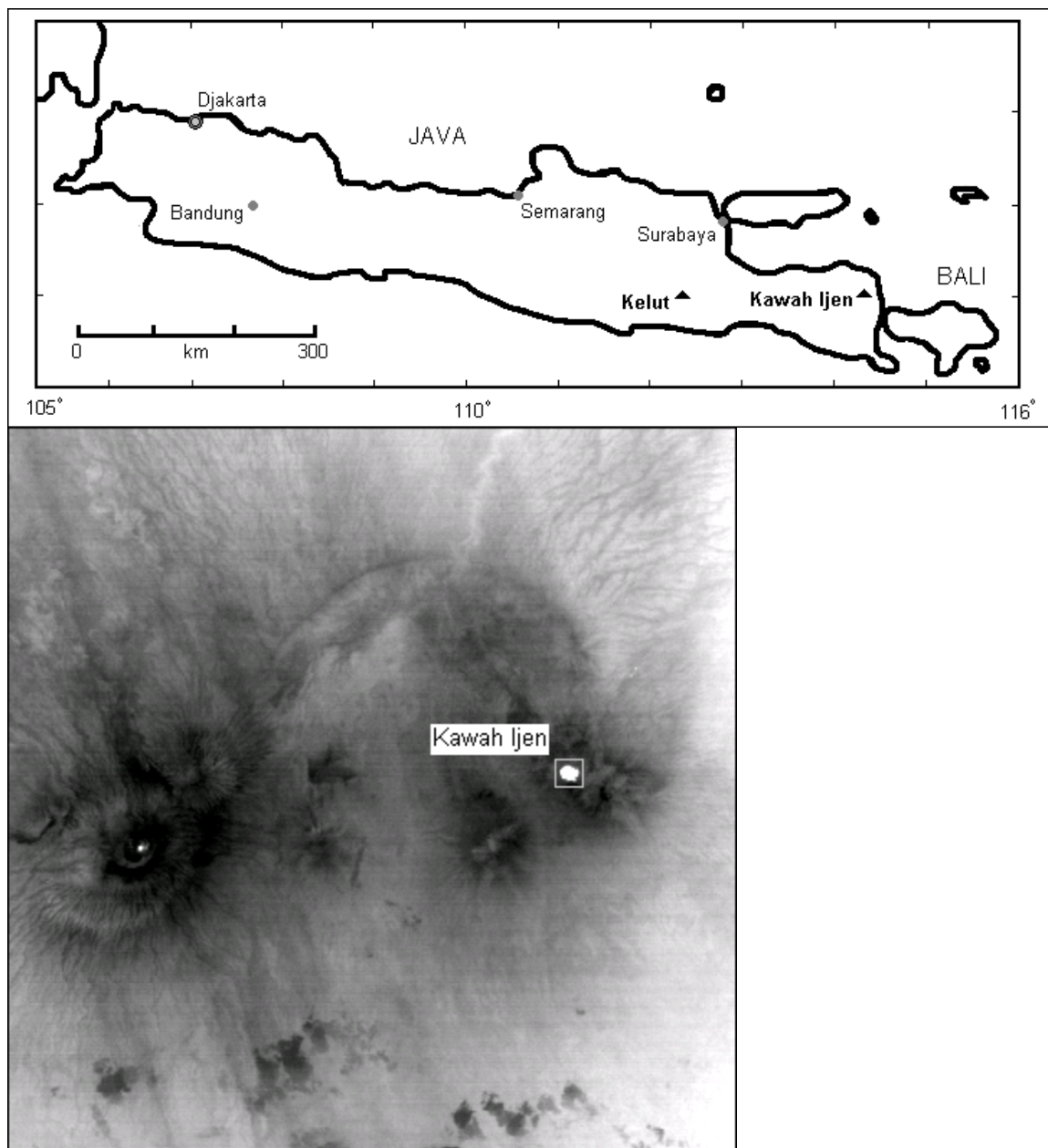
Figure 5.6 a) Map showing the location of Kawah Ijen volcano in Indonesia b) ASTER image of Indonesia's Kawah Ijen volcano, showing the large summit crater lake in the box.

Table 5.4 Images of Kawah Ijen volcano's crater lake, the average temperature of the three hottest lake pixels taken from the AST04 Brightness Temperature Product for each and the temperature calculated using the split-window method. The notation "sl. cl." in the notes column indicates an image where the crater lake may have been partially obscured by clouds.

Granule ID	Date	Local Time	Center Point (Lat, Lon)	AST04 Temp (ºC) Band 14	AST04 Temp (ºC) Band 13	SW Temp. (ºC)	Notes
SC:AST_L1B.003:2016705390	6-Oct-00	3:12:18 PM	-8.04, 113.97	16.9	19.6	31.0	
SC:AST_L1B.003:2018264584	14-Jul-01	3:00:15 PM	-8.18, 114.54	29.4	30.7	36.3	
SC:AST_L1B.003:2018487406	7-Sep-01	3:04:58 PM	-8.04, 113.94	27.9	29.3	36.8	
SC:AST_L1B.003:2027123942	21-May-02	3:00:03 PM	-8.04, 113.95	32.8	33.6	38.6	
SC:AST_L1B.003:2007128234	30-May-02	2:53:56 PM	-8.18, 114.52	20.6	31.9	39.5	
SC:AST_L1B.003:2007301382	22-Jun-02	2:59:49 PM	-8.03, 114.00	29.1	30.9	39.5	
SC:AST_L1B.003:2007921602	24-Jul-02	3:00:01 PM	-8.04, 113.94	29.5	30.8	38.3	
SC:AST_L1B.003:2008207982	9-Aug-02	2:59:48 PM	-7.99, 114.30	30.5	31.4	37.2	
SC:AST_L1B.003:2008368905	25-Aug-02	2:59:53 PM	-7.99, 114.27	28.2	29.0	34.1	
SC:AST_L1B.003:2008763864	12-Oct-02	2:59:18 PM	-8.03, 114.05	27.8	28.9	35.4	
SC:AST_L1B.003:2008903328	28-Oct-02	2:59:29 PM	-8.03, 113.99	25.6	27.0	34.3	
SC:AST_L1B.003:2025311902	4-Nov-02	2:48:20 AM	-8.03, 114.47	24.5	26.2	34.6	
SC:AST_L1B.003:2015060427	25-Jun-03	2:58:21 PM	-8.04, 113.97	12.8	13.4	17.8	
SC:AST_L1B.003:2015313123	11-Jul-03	2:57:53 PM	-7.98, 114.36	31.6	33.4	42.1	
SC:AST_L1B.003:2016327945	12-Aug-03	2:57:32 PM	-8.02, 114.08	33.8	34.6	40.5	
SC:AST_L1B.003:2016766495	28-Aug-03	2:57:38 PM	-8.02, 114.11	31.7	33.0	40.3	
SC:AST_L1B.003:2024084755	26-May-04	2:58:22 PM	-8.03, 114.01	31.0	32.8	43.5	sl. cl.
SC:AST_L1B.003:2024691757	27-Jul-04	2:58:02 PM	-8.03, 114.03	23.1	25.3	35.4	
SC:AST_L1B.003:2025052546	13-Jul-04	2:58:05 PM	-7.99, 114.32	30.0	32.9	46.2	
SC:AST_L1B.003:2025204343	29-Jul-04	2:58:01 PM	-7.99, 114.30	39.1	39.9	45.7	
SC:AST_L1B.003:2025331346	14-Aug-04	2:57:50 PM	-8.03, 114.00	35.3	36.2	42.2	
SC:AST_L1B.003:2027749436	6-Feb-05	2:57:34 PM	-8.02, 114.07	34.3	35.5	42.2	
SC:AST_L1B.003:2028750769	27-Apr-05	2:57:58 PM	-8.03, 114.00	30.4	31.8	39.0	
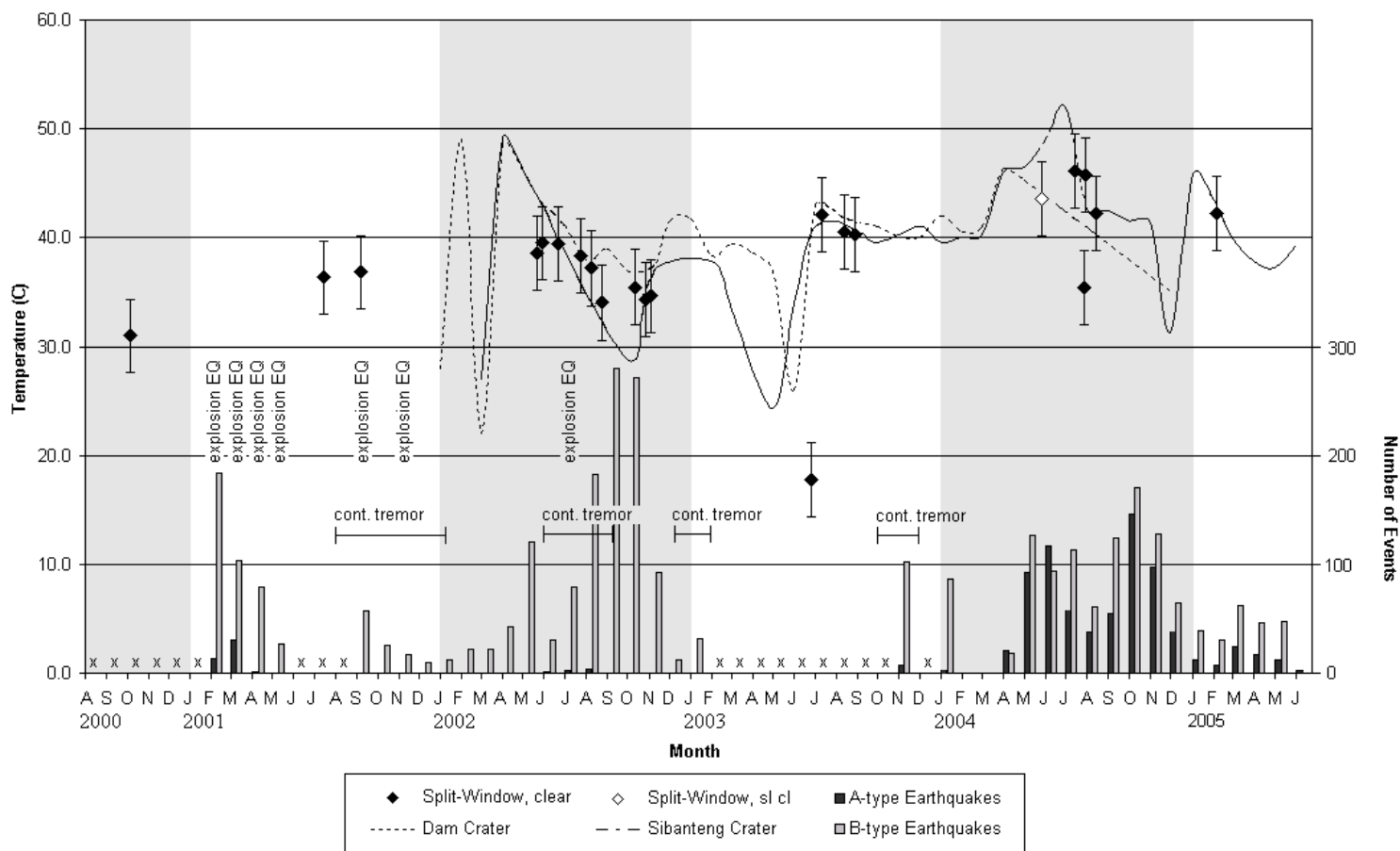
Figure 5.7 Thermal history of Kawah Ijen's crater lake from Oct. 2000 – Apr. 2005. Split-window algorithm results are shown as closed diamonds for clear images and open diamonds for partly cloudy images. Dam Crater and Sibenteng Crater (different locations within the active crater) ground data courtesy of D. Ahmad (pers. commun., 2005). Seismic data is taken from reports of the Global Volcanism Program (Smithsonian, 2005c).
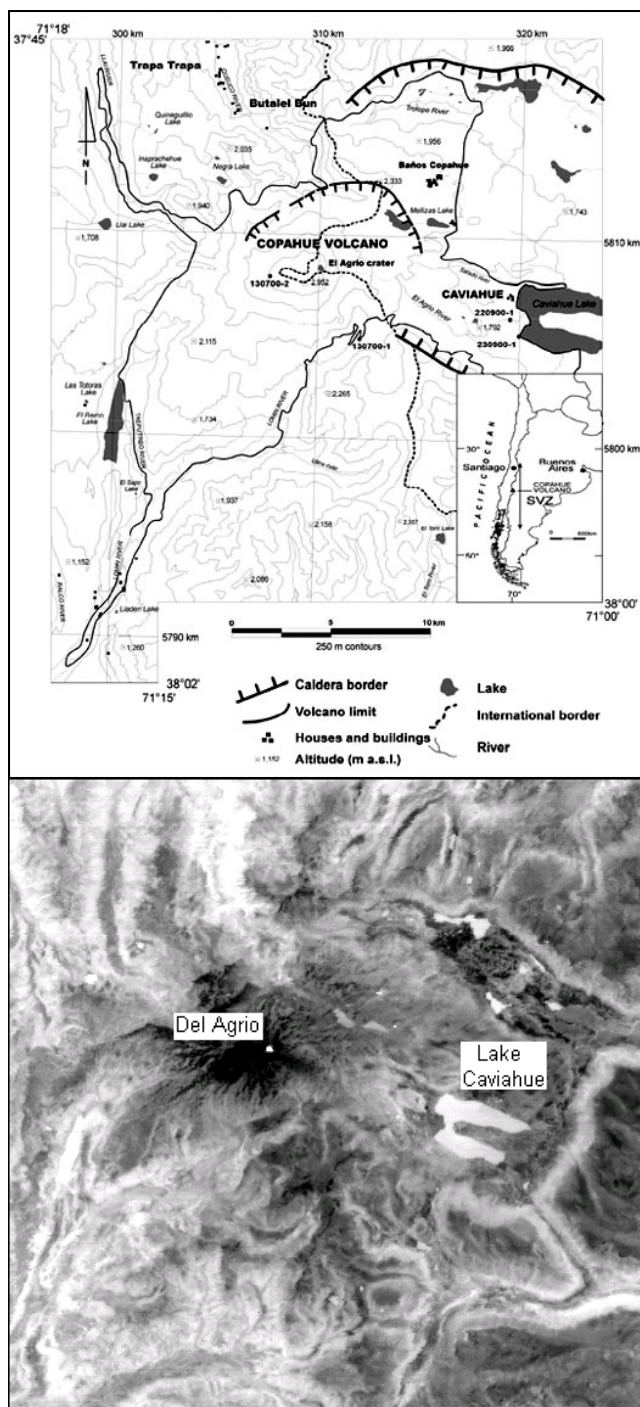
Figure 5.8 a) Map showing the main features of Copahué volcano. Inset shows the location of Copahué within Argentina (Naranjo and Polanco, 2004). b) Thermal ASTER image of Copahué, with the Del Agrio crater lake visible at the summit and glacial Lake Caviahue to the east of the volcano. North is toward the top in this image.

Table 5.5 Images of Copahué volcano's Del Agrio crater lake, the temperature of the hottest lake pixels taken from the AST04 Brightness Temperature Product for each and the temperature calculated using the split-window method.

Granule ID	Date	Local Time	Center Point (Lat, Lon)	AST04 Temp (ºC) Band 14	Band 13	SW Temp (ºC)
SC:AST_L1B.003:2010410577	23-Feb-01	3:54:12 AM	-37.83, -71.48	34.2	35.1	40.8
SC:AST_L1B.003:2007073312	24-Dec-01	3:45:39 AM	-37.82, -71.45	42.9	44.9	55.6
SC:AST_L1B.003:2009790447	11-Dec-02	3:44:05 AM	-37.77, -71.12	37.9	39.7	49.7
SC:AST_L1B.003:2030020902	22-Sep-02	2:47:40 PM	-37.75, -71.36	26.3	27.3	33.7
SC:AST_L1B.003:2010726664	12-Jan-03	3:43:28 AM	-37.81, -71.38	39.0	41.7	54.7
SC:AST_L1B.003:2011901807	22-Feb-03	3:37:18 AM	-37.99, -71.06	44.9	46.3	54.6
SC:AST_L1B.003:2030021218	9-Apr-03	2:53:04 PM	-38.02, -71.04	39.0	40.8	50.4
SC:AST_L1B.003:2013426002	4-May-03	3:42:46 AM	-37.81, -71.38	5.4	8.7	23.6
SC:AST_L1B.003:2015437773	16-Jul-03	3:35:47 AM	-38.04, -71.43	19.8	24.0	42.9
SC:AST_L1B.003:2030021224	15-Aug-03	2:51:39 PM	-38.00, -71.19	29.5	31.7	42.9
SC:AST_L1B.003:2016723821	24-Aug-03	3:41:53 AM	-37.80, -71.32	24.2	25.8	34.0
SC:AST_L1B.003:2019529582	30-Dec-03	3:43:42 AM	-37.79, -71.19	10.9	13.4	25.2
SC:AST_L1B.003:2030020918	22-Jan-04	2:53:14 PM	-37.98, -71.36	31.1	31.6	35.7
SC:AST_L1B.003:2030020925	27-Apr-04	2:52:27 PM	-38.00, -71.22	11.0	11.4	14.4
SC:AST_L1A.003:2021422898	22-Mar-05	2:53:14 PM	-37.98, -71.35	23.3	25.8	37.6
SC:AST_L1B.003:2028705274	23-Apr-05	3:42:14 AM	-37.76, -71.03	16.4	21.1	41.8
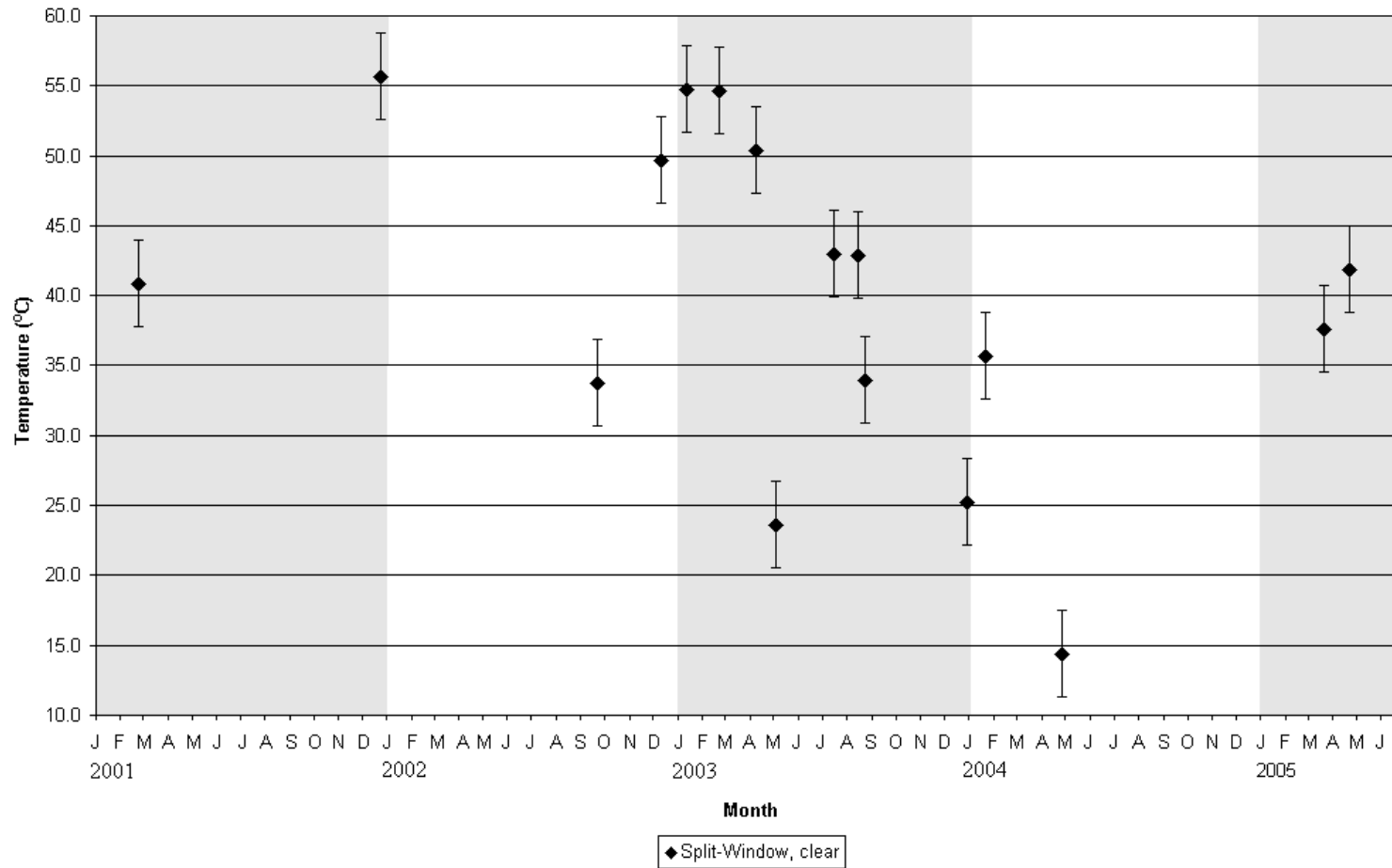
Figure 5.9 Thermal history of Copahué's crater lake from Feb. 2001 – Apr. 2005.

6. Conclusion

An innovative application of remote sensing is the measurement of crater lake water temperatures from space, using the ASTER instrument flown on NASA's Terra satellite platform. The benefits of remote sensing become clear when one considers the difficulty and expense, as well as the danger, involved in making such measurements using traditional methods. Crater lake temperatures are useful for monitoring volcanic activity, in addition to other techniques, such as monitoring lake chemistry, seismic activity, and deformation. This is due to the fact that magma at depth interacts with the hydrothermal systems of volcanoes, and influences the temperature of the crater lake, which is a surface expression of the hydrothermal system. Crater lake temperatures have served as warnings prior to eruptions in the past, as an increase in heat flux translates to an overall increase in lake temperatures, the lake playing the role of a calorimeter in the system.

Numerous volcanoes exist for which satellite-based temperature observations may be useful, since a significant percentage of the world's active volcanoes contain crater lakes. Given the potential utility of this method, a disappointing number of ASTER images are available for active volcanoes with crater lakes from which to calculate water temperatures. However, enough images were available for at least 6 different volcanoes to make headway on this approach. First, data for Taal volcano was analyzed in order to develop a split-window algorithm for calculating lake water temperatures. The split-window algorithm is necessary In order to produce reasonably accurate temperature data

from ASTER imagery, because atmospheric effects must first be removed from the data.

Then, data from Kusatsu-Shirane volcano, where a wealth of corresponding ground-data

is available, was used to validate the split-window approach. The results may be viewed

in light of fieldwork that explored how the radiant temperatures, which may be measured

from space, relate to the bulk temperature of the lake. Finally, a thermal history for the

crater lake on Copahué volcano was established, where few previous temperature

measurements exist. Temperature calculations were also successfully made for the crater

lakes of Ruapehu, Poás, and Kawah Ijen volcanoes, all of which exist under different

conditions than the crater lake of Taal volcano, for which the split-window algorithm was

originally developed, demonstrating its widespread utility. Errors in the temperature

measurements are on the order of tens of degrees Celsius, which means that the data are

sufficient for observing temperature increase of crater lakes, which tend to be on the

order of several degrees Celsius.

To conclude, the goals of this project, to develop a method for calculating water

temperatures in crater lakes on active volcanoes using ASTER thermal imagery, and to

learn something about the thermal history of crater lakes during periods of volcanic

activity, was reached. Thermal histories were charted for four volcanoes: Ruapehu,

Poás, Kawah Ijen, and Copahué, over the years 2000 to 2005. In the first three cases,

temperature measurements were compared to available ground data and the temperature

measurements were found to be reliable. In each of the cases where other monitoring

data was available, temperature increases were observed that corresponded to increases in

seismic and other activity. In most instances, increases in lake water temperatures

preceded the onset of increased seismic activity by several months. Therefore, increases in water temperatures measured by ASTER might serve as an early warning sign for new activity. Also, the thermal time-series that were produced are complete enough in some cases to serve as a substitute for in-situ temperature measurements, should the situation warrant. In the case of Copahué volcano, results from the split-window algorithm provide a thermal record for the crater lake where none would otherwise exist. This may be useful in the future to establish background lake temperature trends, which may aid in understanding new episodes of warming.

References

M. Abrams, S. Hook, B. Ramachandran, 2002. ASTER User Handbook: Version 2.

R.E. Alley and M. Jentoft-Nilsen, 1999. Algorithm Theoretical Basis Document for Brightness Temperature: Version 3.0.

M. Badrudin, 1994. Kelut volcano monitoring: Hazards, mitigation and changes in water chemistry prior to the 1990 eruption. Geochemical Journal, 28: 233-241.

S.L. Brantley, G.L. Rowe, L.F. Konikow, and W.E. Sanford, 1992. Toxic Waters of Poás Volcano. National Geographic Research and Exploration, 8 (3): 328-337.

S.L. Brantley, A.M. Ágústsdóttir, and G.L. Rowe, 1993. Crater Lakes Reveal Volcanic Heat and Volatile Fluxes. GSA Today, 3 (7): 175-178.

G. Brown, H. Rymer, J. Dowden, P. Kapadia, D. Stevenson, J. Barquero, and L.D. Morales, 1989. Energy Budget Analysis for Poás Crater Lake: Implications for Predicting Volcanic Activity. Nature, 339: 370-373.

G.C. Brown, H. Rymer, and D. Stevenson, 1991. Volcano Monitoring by Microgravity and Energy Budget Analysis. Journal of the Geological Society, London, 148: 585-593.

L. Casertano, A. Borgia, C. Cigolini, L.D. Morales, W. Montero, M. Gomez, and J.F. Fernandez, 1987. An Integrated Dynamic Model for the Volcanic Activity at Poás Volcano, Costa Rica. Bulletin of Volocanology, 49: 588-598.

B.W. Christenson, 1994. Convection and Stratification in Ruapehu Crater Lake, New Zealand: Implications for Lake Nyos-Type Gas Release Eruptions. Geochemical Journal, 28: 185-197.

B.W. Christenson, 2000. Geochemistry of fluids associated with the 1995-1996 eruption of Mt. Ruapehu, New Zealand: Signatures and processes in the magmatic-hydrothermal system. Journal of Volcanology and Geothermal Research, 97: 1-30.

P. Dash, F.M. Göttsche, F.S. Olesen, and H. Fischer, 2002. Land Surface Temperature and Emissivity Estimation from Passive Sensor Data: Theory and Practice – Current Trends. International Journal of Remote Sensing, 23 (13): 2563-2594.

H. Fujisada, K. Arai, K. Fukue, A. Iwasaki, M. Kaku, F. Sakuma, I. Sato, M. Urai, H. Watanabe, and M. Kato, 1996. Algorithm Theoretical Basis Document for ASTER Level-1 Data Processing: Version 3.0.

W. Giggenbach, 1974. The Chemistry of Crater Lake, Mt. Ruapehu (New Zealand) During and After the 1971 Active Period. New Zealand Journal of Science, 17: 33-45.

L. Hasse, 1971. The Sea Surface Temperature Deviation and the Heat Flow at the Sea-Air Interface. Boundary-Layer Meteorology, 1: 368-379.

S.L. Hook, F.J. Prata, R.E. Alley, A. Abtahi, R.C. Richards, S.G. Schladow, and S.O. Pálmarsson, 2003. Retrieval of Lake Bulk and Skin Temperatures Using Along-Track Scanning Radiometer (ATSR-2) Data: A Case Study Using Lake Tahoe, California. Journal of Atmospheric and Oceanic Technology, 20: 534-548.

B.F. Houghton, J.H. Latter, W.R. Hackett, 1987. Volcanic hazard assessment for Ruapehu composite volcano, Taupo Volcanic Zone, New Zealand. Bulletin of Volcanology, 49: 737-751.

A.W. Hurst, H.M. Bibby, B.J. Scott, and M.J. McGuinness, 1991. The heat source of Ruapehu Crater Lake; deductions from the energy and mass balances. Journal of Volcanology and Geothermal Research, 46: 1-20.

A.W. Hurst and R.R. Dibble, 1981. Bathymetry, Heat Output and Convection in Ruapehu Crater Lake, New Zealand. Journal of Volcanology and Geothermal Research, 9: 215-236.

A.W. Hurst and P.J. McGinty, 1999. Earthquake Swarm to the West of Mt. Ruapehu Preceding its 1995 Eruption. Journal of Volcanology and Geothermal Research, 90: 19-28.

A.W. Hurst, 1998. Shallow Seismicity Beneath Ruapehu Crater Lake: Results of a 1994 Seismometer Deployment. Bulletin of Volcanology, 60: 1-9.

Institute of Geological and Nuclear Sciences (2005). Hazard Watch Science Alert Bulletins.

M. Kusakabe, 1996. Hazardous crater lakes. In R. Scarpa and R.I. Tilling (Eds.) Monitoring and Mitigation of Volcano Hazards. Springer, Berlin: 573-598.

S. Lesage, 1995. Seismic Precursors of the February 10, 1990 Eruption of Kelut Volcano, Java. Journal of Volcanology and Geothermal Research, 65: 135-146.

M. Martínez, E. Fernández, J. Valdéz, V. Barboza, R. Van der Laat, E. Duarte, E. Malavassi, L. Sandoval, J. Barquero, and T. Marino, 2000. Chemical Evolution and Volcanic Activity of the Active Crater Lake of Poás Volcano, Costa Rica, 1993-1997. Journal of Volcanology and Geothermal Research, 97: 127-141.

L.M. McMillin, 1975. Estimation of Sea Surface Temperatures from Two Infrared Window Measurements with Different Absorption. Journal of Geophysical Research, 80 (36): 5113-5117.

P.J. Mouginis-Mark and N. Domergue-Schmidt, 2000. Acquisition of Satellite Data for Volcano Studies. Remote Sensing of Active Volcanism, Geophysical Monograph 116: 9-24.

J.A. Naranjo and E. Polanco, 2004. The 2000 AD Eruption of Copahué Volcano, Southern Andes. Revista Geológica de Chile, 31 (2): 279-292.

S. Neshyba, W. Fernandez, and J. Diaz-Andrade, 1988. Temperature Profiles from Poás Crater Lake. Eos Transactions, 69 (19).

E.G. Njoku, 1990. Satellite Remote Sensing of Sea Surface Temperature. In G.L. Geernaert and W.J. Plant (Eds.) Surface Waves and Fluxes: Volume II – Remote Sensing. Kluwer Academic Publishers, Dordrecht: 311-338.

T. Ohba, J. Hirabayashi, K. Nogami, 1994. Water, heat and chloride budgets of the crater lake, Yugama at Kusatsu-Shirane volcano, Japan. Geochemical Journal, 28: 217-231.

T. Ohba, J. Hirabayashi, and K. Nogami, 2000. D/H and $^{18}O/^{16}O$ Ratios of Water in the Crater Lake at Kusatsu-Shirane Volcano, Japan. Journal of Volcanology and Geothermal Research, 97: 329-346.

C. Oppenheimer, 1993. Infrared surveillance of crater lakes using satellite data. Journal of Volcanology and Geothermal Research, 55: 117-128.

C. Oppenheimer, 1996. Crater Lake Heat Losses Estimated by Remote Sensing. Geophysical Research Letters. 23 (14): 1793-1796.

C. Oppenheimer, 1997a. Ramifications of the Skin Effect for Crater Lake Heat Budget Analysis. Journal of Volcanology and Geothermal Research, 75: 159-165.

C. Oppenheimer, 1997b. Remote Sensing of the Colour and Temperature of Volcanic Lakes. International Journal of Remote Sensing, 18 (1): 5-37.

G.B. Pasternack, J.C. Varekamp, 1997. Volcanic lake systematics I. Physical constraints. Bulletin of Volcanology, 58: 528-538.

D. Pieri, M. Abrams, 2004. ASTER Watches the World's Volcanoes: A New Paradigm for Volcanological Observations from Orbit. Journal of Volcanology and Geothermal Research, 135: 13-28.

I.S. Robinson, N.C. Wells, and H. Charnock, 1984. The Sea Surface Thermal Boundary Layer and its Relevance to the Measurement of Sea Surface Temperature by Airborne and Spaceborne Radiometers. International Journal of Remote Sensing, 5 (1): 19-45.

G.L. Rowe, S.L. Brantley, M. Fernandez, J.F. Fernandez, A. Borgia, and J. Barquero, 1992. Fluid-volcano interaction in an active stratovolcano: The crater lake system of Poás volcano, Costa Rica. Journal of Volcanology and Geothermal Research, 49: 23-51.

H. Rymer, J. Cassidy, C.A. Locke, M.V. Barboza, J. Barquero, J. Brenes, R. Van der Laat, 2000. Geophysical studies of the recent 15-year eruptive cycle at Poás Volcano, Costa Rica. Journal of Volcanology and Geothermal Research, 97: 425-442.

J.W. Salisbury and D.M. D'Aria, 1992. Emissivity of Terrestrial Materials in the 8-14 μm Atmospheric Window. Remote Sensing of Environment, 42: 83-106.

B.J. Scott, 1991. A simple method for continuously recording the temperature of Crater Lake, Mt. Ruapehu. New Zealand Geological Survey Record, 43: 51-55.

J.B. Shepherd and H. Sigurdsson, 1978. The Soufriére Crater Lake as a Calorimeter. Nature, 271: 344-345.

L. Siebert and T. Simkin (2002-). Volcanoes of the World: an Illustrated Catalog of Holocene Volcanoes and their Eruptions. Smithsonian Institution, Global Volcanism Program, Digital Information Series, GVP-3, (http://www.volcano.si.edu/world/).

Smithsonian Institution (2005a). Ruapehu. Bulletin of the Global Volcanism Network.

Smithsonian Institution (2005b). Poás. Bulletin of the Global Volcanism Network.

Smithsonian Institution (2005c). Kawah Ijen. Bulletin of the Global Volcanism Network.

Smithsonian Institution (2005d). Copahué. Bulletin of the Global Volcanism Network.

H. Tonooka, F. Sakuma, M. Kudoh, and K. Iwafune. ASTER/TIR Onboard Calibration Status and User-Based Recalibration, 2004. Proceedings of SPIE, 5234: 191-201.

H. Tsuya, 1932. Explosive Activity of Volcano Kusatsu-Sirané in October, 1932. Bulletin of the Earthquake Research Institute, 11: 82-117.

J. Vandemeulebrouck, J.C. Sabroux, M. Halbwachs, Surono, N. Poussielgue, J. Grangeon, J. Tabbagh, 2000. Hydroacoustic Noise Precursors of the 1990 Eruption of Kelut Volcano, Indonesia. Journal of Volcanology and Geothermal Research, 97: 443-456.

J.C. Varekamp, A.P. Ouimette, S.W. Herman, A. Bermúdez, and D. Delpino, 2001. Hydrothermal Element Fluxes from Copahué, Argentina: A "Beehive" Volcano in Turmoil. Geology, 29 (11): 1059-1062.

Y. Yamaguchi, A.B. Kahle, H. Tsu, T. Kawakami, and M. Pniel, 1998. Overview of Advanced Spaceborne Thermal Emission and Reflection Radiometer (ASTER). IEEE Transactions on Geoscience and Remote Sensing, 36 (4): 1062-1071.